



## UvA-DARE (Digital Academic Repository)

### Bending benzenes and twisting light

Kovida, K.

**Publication date**  
2026

[Link to publication](#)

#### **Citation for published version (APA):**

Kovida, K. (2026). *Bending benzenes and twisting light*. [Thesis, fully internal, Universiteit van Amsterdam].

#### **General rights**

It is not permitted to download or to forward/distribute the text or part of it without the consent of the author(s) and/or copyright holder(s), other than for strictly personal, individual use, unless the work is under an open content license (like Creative Commons).

#### **Disclaimer/Complaints regulations**

If you believe that digital publication of certain material infringes any of your rights or (privacy) interests, please let the Library know, stating your reasons. In case of a legitimate complaint, the Library will make the material inaccessible and/or remove it from the website. Please Ask the Library: <https://uba.uva.nl/en/contact>, or a letter to: Library of the University of Amsterdam, Secretariat, P.O. Box 19185, 1000 GD Amsterdam, The Netherlands. You will be contacted as soon as possible.

# 4

## Effect of $\pi$ -Electron Conjugation on the Chiroptical Properties of Helicene Carbon Nanohoops

---

This chapter has been published as: Kovida K.; Malinčík J.; Šolomek T. Effect of  $\pi$ -Electron Conjugation on the Chiroptical Properties of Helicene Carbon Nanohoops. *Helv. Chim. Acta* **2025**, *108*, e202400166.

## Abstract

In this chapter, we designed, synthesized, and investigated a new chiral carbon nanohoop that formally incorporates a benzothiadiazole and [5]helicene units into the structure of [6]cycloparaphenylene. The connection of these units in the chiral nanohoop is designed to allow for  $\pi$ -electron conjugation between the benzothiadiazole chromophore and the chirality-inducing [5]helicene. We resolved the enantiomers of the highly fluorescent, near-IR light emitting benzothiadiazole helicene nanohoop. Electronic circular dichroism spectroscopy then allowed us to investigate whether the selected molecular design leads to an increase in the lowest singlet excited state delocalization to improve the compound's electronic dissymmetry factor in comparison to the previously studied benzothiadiazole carbon nanohoop with planar chiral [2.2]paracyclophane unit with *pseudo-para* connection.

## 4.1 Introduction

Chirality is a fundamental concept in chemistry<sup>1-3</sup> and has been investigated in several systems. Besides the fundamental fascination, chirality controls a significant part of biology,<sup>4</sup> finds applications in photonics,<sup>5-8</sup> or it induces spin polarization in transmitted or emitted electrons.<sup>9,10</sup>

In photonics, chiral materials exhibit unique optical properties, such as different interaction of enantiomers with circularly polarized light at absorption, *e.g.*, circular dichroism (CD), or emission, circularly polarized luminescence (CPL). The development of chiral materials, which can selectively absorb or emit circularly polarized light, opens opportunities to advance optoelectronic devices,<sup>11</sup> sensor technologies,<sup>12</sup> and information processing systems.<sup>13</sup>

Chirality is not directly quantifiable, and one molecule cannot be regarded as more chiral than another. Yet chemists often strive to “measure” chirality by quantifying its physical consequences. Among the variety of available techniques, electronic circular dichroism (ECD) spectroscopy<sup>14</sup> offers high sensitivity and ability to provide insights into the structure and stereochemical properties of chiral molecules. An enantiomer possesses a different absorption cross-section for left- and right-handed circularly polarized light. Therefore, a common measure used in ECD to characterize novel chiral aromatics which determines this difference is  $\Delta\epsilon$ , is defined as:

$$\Delta\epsilon = \epsilon_L - \epsilon_R \quad \text{eq. 1}$$

where  $\epsilon_L$  and  $\epsilon_R$  are the molar decadic absorption coefficients measured for the absorption of left- and right-handed circularly polarized light, respectively. The resulting  $\Delta\epsilon$  is a direct measure of the chiroptical activity. However, it often depends strongly on factors that affect the overall absorption of the molecule, such as solvent polarity, pH, or temperature. In addition,  $\Delta\epsilon$  alone makes direct comparisons to assess different chiral chromophores challenging. For example,  $\Delta\epsilon$  for the Cotton effect at the 0–0 transition in a series of helicene nanoribbons made of perylene diimides (PDIs) increases with their molecular length.<sup>15,16</sup> But it merely reflects the number of individual PDI chromophores in the nanoribbon. As correctly pointed out by Nuckolls and co-workers in this case, the electronic absorption dissymmetry factor  $g_{abs}$  represents a better “measure” of chirality, and a similar figure of merit,  $g_{lum}$ , is widely accepted in the research of circularly polarized luminescence.<sup>17</sup>

The dissymmetry factor  $g_{abs}$  is defined in eq. 2:

$$g_{abs} = \frac{2(A_L - A_R)}{A_L + A_R} \quad \text{eq. 2}$$

where  $A_L$  and  $A_R$  are the absorbance values for the left- and right-handed circularly polarized light, respectively. Analogously, one can replace the absorbances for individual intensities of the emitted light to obtain  $g_{lum}$ . These factors in absolute value range from 0 to 2, normalize the absorption/emission differences, and provide a dimensionless scale for comparing variety of chiral systems. The closer the value of  $g$  to 2, the stronger the chiroptical response. Dissymmetry factors thus offer a robust and reliable approach for quantifying and studying chirality.<sup>18</sup> Although environmental factors still affect the value of  $g$ , it is less sensitive to experimental changes, improving reproducibility of measurements across various setups. The  $g$  can also be described by equation 3, which enables an effective interpretation of experimental chiroptical data with molecular electronic transitions obtained with the help of theoretical calculations:

$$g = 4 \frac{|\mu_{ij}| |m_{ij}| \cos \theta}{|\mu_{ij}|^2 + |m_{ij}|^2} \quad \text{eq. 3}$$

where  $\mu_{ij}$  and  $m_{ij}$  are electric and magnetic transition dipole moment, respectively, for a transition between  $i$ -th and  $j$ -th state and  $\theta$  is the angle between them. The expression is valid equally for the ECD or CPL.

Among chiral aromatic molecules, [2.2]paracyclophane<sup>19–21</sup> ([2.2]PCP) and [ $n$ ]carbohelicenes<sup>22–24</sup> are arguably the most studied systems.<sup>1–3,25</sup> However, none of these molecules alone represents a good, tunable fluorophore with a high luminescence quantum yield ( $\phi_{lum}$ ).<sup>26,27</sup> But paracyclophanes<sup>21,28–30</sup> and helicenes<sup>16,31–39</sup> can be embedded into larger nanostructures<sup>40,41</sup> and exhibit high quantum yields. However, the dissymmetry factor  $g_{lum}$  is usually low.

A particularly interesting subset of chiral aromatic systems are hoop-like macrocycles. They may adopt rigid structures to achieve a configurationally stable chiral conformations or they may also incorporate a chiral unit. Macrocycles do not possess a terminus, which permits to achieve structures with high symmetry to control transition dipole moments. In addition, they can bear a cavity to interact with molecular guests.

However, only a few examples of chiral macrocycles that display large values of  $g$ , in particular in CPL, are known.<sup>46–48</sup> A faster progress in development of suitable chiral systems is hampered by the absence of a clear set of molecular design guidelines,<sup>49–52</sup> although the underlying theory of the molecule–light interaction is well understood.<sup>14</sup> Among the few known rules, imposing symmetry to the chiral system may lead to enhancement of the value of  $g$ , as showed for  $g_{lum}$  in the figure-eight-shaped [5]helicene dimer studied by Matsuda and Hirose.<sup>51</sup> Generally, molecules that belong to  $D_n$  or  $C_n$  point groups of symmetry allow to ideally align  $\mu$  and  $m$  transition moments (see eq.3).<sup>46,53</sup> However, a high symmetry often compromises the size  $|\mu|$  and thus diminishes  $\varepsilon$  or  $\phi_{lum}$  by decreasing the luminescence rate constant. Recently, a link between the area of the inner cavity of a chiral macrocyclic structure and  $|m|$  has been elucidated computationally with the help of machine learning.<sup>52</sup> Crassous and Favereau showed how excitonically-coupled chromophores and excited state symmetry-breaking affected the  $g_{lum}$  in an acyclic  $\pi$ -helical system.<sup>33,35</sup> This important work underscores a critical aspect of the excited states involved in the chiroptical response that remains underappreciated in the literature. Excitonic coupling requires that the excited state is delocalized among the coupled chromophores. The same can be argued about excited states with a high symmetry imposed on them.

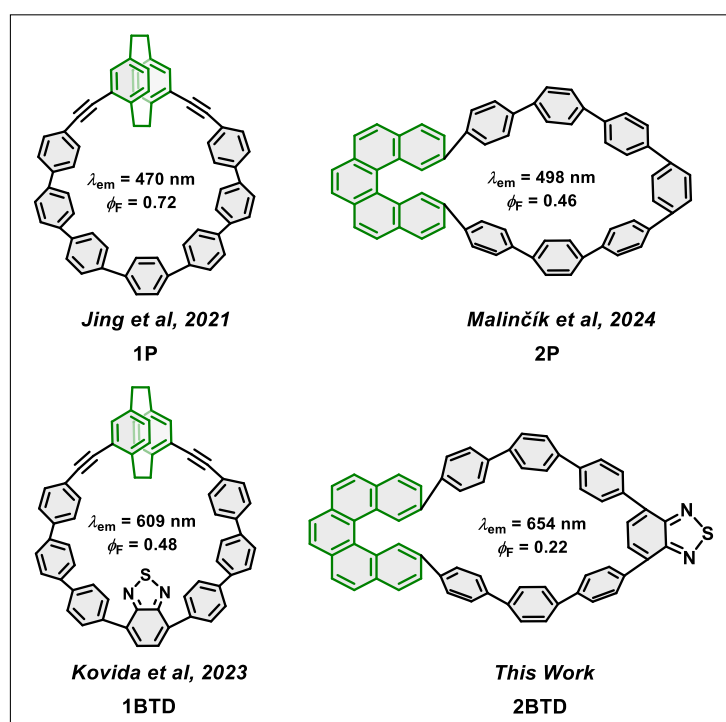


**Figure 4.1.** Chiral nanohoops with [2.2]PCP<sup>42–44</sup> or [5]helicene<sup>45</sup> chiral units and a segment of seven *para*-phenylenes (eventually modified with benzothiadiazole).

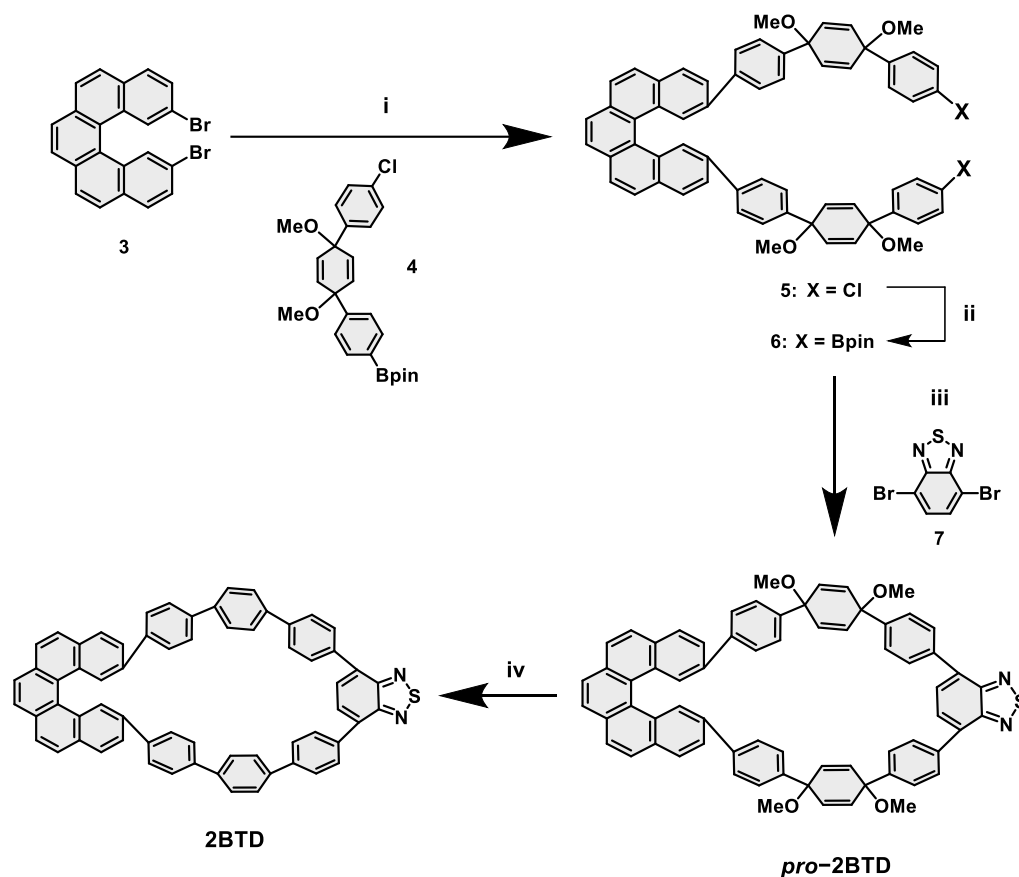
Therefore, in our recent study,<sup>54</sup> we tested the effect of a stepwise exciton localization to benzothiadiazole (BTD) on the change in the chiroptical response between macrocycles **1P** and **1BTD** (Figure 4.1). Thereby, we succeeded in extending the few existing design guidelines and emphasized that the requirement of a high symmetry, which restricts the available compound design space, is useful but not a prerequisite to achieve a strong chiroptical response ( $g_{\text{abs}}$ ) in a chiral system. For example, changing the connection of [2.2]PCP in the nanohoop from *pseudo-meta* in **1P** to *pseudo-para* predicted a large boost in  $g_{\text{abs}}$ . However, the corresponding nanohoop is not configurationally stable to verify this prediction.<sup>43</sup>

Therefore, in the present study, we investigate a model **2BTD** (Figure 4.1) with  $\pi$ -electron conjugation between the BTD chromophore<sup>55</sup> and a different chirality-inducing unit, namely [5]helicene. We selected [5]helicene connected via its 9,12-positions to replace the *pseudo-meta* [2.2]PCP in **1BTD** because it enables to mix its frontier molecular orbitals (MOs) with those on the curved *para*-phenylene segment, unlike in *pseudo-meta* [2.2]PCP or [6]helicene.<sup>45,56</sup> The corresponding carbon nanohoop **2P** was previously synthesized by us and others<sup>45,57</sup> and proved to possess configurational stability to resolve and investigate individual enantiomers at room temperature. We expected that incorporation of the BTD unit would allow us to investigate whether and how the BTD–helicene conjugation impacts the exciton (de)localization and the dissymmetry factor  $g_{\text{abs}}$  that we use here also as the proxy for the  $g_{\text{lum}}$ . Thereby, we accomplished synthesis of a new chiral carbon nanohoop and its precursor *pro-2BTD* (Scheme 4.1) with large Stokes shifts and relatively bright fluorescence that extends well into the near-IR region.

## 4.2 Results and Discussion

The synthesis of the target chiral nanohoop **2BTD** is depicted in Scheme 4.1. Suzuki-Miyaura cross-coupling reaction of 9,12-dibromo-[5]helicene **3**<sup>58</sup> and compound **4**<sup>59</sup> synthesized according to Jasti and co-workers was afforded **5** in 80% yield. Compound **5** was subsequently transformed via Miyaura borylation to form the corresponding diboronate ester **6**.<sup>45</sup> Suzuki-Miyaura cross-coupling reaction of **6** with 4,7-dibromo-benzothiadiazole **7** resulted in the remarkably clean formation of the macrocyclic precursor of the target compound *pro-2BTD* as the sole product. The crude *pro-2BTD* product was purified by passing the reaction mixture through a short pad of silica followed by gel permeation chromatography (GPC) using chloroform as eluent. The macrocycle was obtained in 56% yield as a crystalline yellow solid exhibiting bright green fluorescence in solution and yellow fluorescence in solid state. We observed no decomposition of

the sample during purification or upon its storage as a solid material at ambient temperature, although in some cases, the pro-aromatic cyclohexa-1,4-dienes tend to undergo rearrangements in  $\text{CHCl}_3$  or even in the solid state.<sup>54,56,60</sup>



**Scheme 4.1.** Synthesis of **2BTd**. Reaction conditions: (i) 2 equiv. of **4**, 0.1 equiv. of Pd SPhos G3, 8 equiv. of  $\text{K}_3\text{PO}_4$ , dioxane: $\text{H}_2\text{O}$  = 10:1, room temperature, 24 h, 80%; (ii) 4 equiv. of  $(\text{Bpin})_2$ , 6.6 equiv. of KOAc, 0.05 equiv. of  $\text{Pd}_2\text{dba}_3$ , 0.2 equiv. of XPhos, dioxane, 80 °C, 16 h; (iii) 1.1 equiv. of **7**, 0.1 equiv. of Pd SPhos G3, 2M aq.  $\text{K}_3\text{PO}_4$ , dioxane: $\text{H}_2\text{O}$  = 10:1, 80 °C, 18 h, 56%; (iv) 9 equiv. of  $\text{H}_2\text{SnCl}_4$ , THF, room temperature, 30 min, 43%.

Nevertheless, the recorded  $^1\text{H}$  NMR spectrum of the purified sample of *pro*-2BTd in  $\text{CDCl}_3$  showed presence of a minor impurity (<5%), which we could not separate by repeating the recycling-GPC. A DOSY NMR experiment of the sample in  $\text{CDCl}_3$  suggests that both compounds in the sample possess nearly identical diffusion coefficient, which proposes that the observed species might represent a minor conformer of *pro*-2BTd. However, variable-temperature  $^1\text{H}$  NMR experiments (80 °C to -50 °C) of a sample of *pro*-2BTd in toluene- $d_8$  did not lead to a coalescence of the resonances, thus providing us with no conclusive evidence.

Subsequently, **pro-2BTD** was treated with a mixture of SnCl<sub>2</sub> and HCl as developed by Yamago<sup>61</sup> and co-workers to accomplish reductive aromatization. Notably, a sudden color change of the reaction mixture from yellow to orange was observed immediately upon the addition of the reductant. In our group's experience, we frequently observe formation of side products because of acid-induced rearrangements during the aromatization of similar compounds. We detected no major side products after optimizing the reaction conditions in this case. Yet, the target nanohoop **2BTD** was isolated by GPC in only moderate 43% yield. The obtained red solid exhibited bright orange-red fluorescence in both solid state and in solution. We observed slow decomposition of **2BTD** in the presence of ambient light and air; however, a longer chemical stability can be achieved by storing the compound in the dark <4 °C. The final compound was fully characterized by NMR spectroscopy and high-resolution mass spectrometry (see the appendix).

**Photophysical properties of target compounds:** We investigated the light absorption and luminescence of **2BTD** and **pro-2BTD** (Table 4.1) to determine the consequence of replacing the [2.2]PCP chiral unit in **1BTD** and **pro-1BTD** by [5]helicene. The corresponding spectra (Figure 4.2, top) were measured at room temperature for samples dissolved in CH<sub>2</sub>Cl<sub>2</sub>.

The characteristic major absorption band for **2BTD** was observed at  $\lambda_{\text{max}} = 328$  nm, close to the typical wavelength of cycloparaphenylenes and related carbon nanohoops.<sup>56,62–64</sup> The absence of a high molecular symmetry leads to another allowed, red-shifted band maximum observed at 479 nm that corresponds to the HOMO–LUMO transition. The nature of this transition is clearly supported by the analysis of the natural transition orbitals (NTOs, Figure 4.3, Table A4.7, Figures A4.16–A4.17) from our DFT calculations. Despite the absence of the two ethynyl units present in nanohoop **1BTD**, the HOMO–LUMO transition in **2BTD** shows a bathochromic shift of  $\sim 1350$  cm<sup>-1</sup> with respect to **1BTD**, although they consist of the same sequence of phenylene and BTD units. The complete turn-off of the  $\pi$ -electron conjugation in **pro-2BTD** by the two cyclohexa-1,4-dienes shifts the HOMO–LUMO transition to 399 nm, mere  $\sim 650$  cm<sup>-1</sup> apart from the analogous transition in **pro-1BTD** (389 nm). Therefore, we attribute the additional shift of  $\sim 700$  cm<sup>-1</sup> to the stabilization of the S<sub>1</sub> excited state in **2BTD** due to increased effective conjugation.

Indeed, the analysis of the frontier molecular orbitals in **2BTD** shows a significant contribution of both BTD and [5]helicene to the HOMO. However, the LUMO does not mix MOs from both units and is largely localized on the *para*-phenylenes containing the electron-poor BTD.

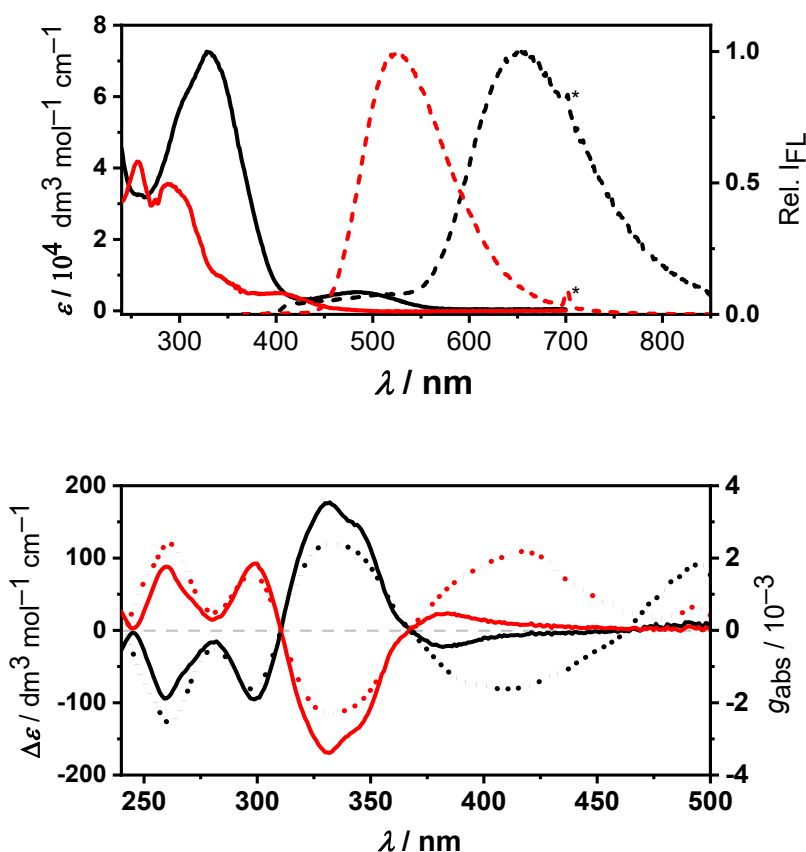


**Figure 4.2.** (top) UV-vis absorption (solid line) and emission (dashed line, excited at 350 nm) spectra of *pro*-2BTD (red) and 2BTD (black). (bottom) ECD (solid line) and  $g_{\text{abs}}$  spectra (dotted line, smoothed, see the appendix for raw data) of (*P*)-2BTD (black) and (*M*)-2BTD (red). All samples in  $\text{CH}_2\text{Cl}_2$  at  $c \sim 1 \times 10^{-5}$  M. \*= scattered light.

The best set of MOs describing the  $S_0 \rightarrow S_1$  transition (Figure 4.3) then shows that the [5]helicene contribution is fully rotated out from the NTOs. Yet, the coefficients on the phenylenes adjacent to the chiral unit are somewhat larger in 2BTD than in 1BTD. A similar  $S_1$  state stabilization in 2BTD can be observed by comparing the luminescence spectra of these compounds (Table 4.1). The fluorescence maximum of 2BTD is observed at impressive  $\lambda_{\text{em}} = 654$  nm and extends markedly to the near-IR region. Again, the absence of  $\pi$ -electron conjugation leads to  $\lambda_{\text{em}} = 526$  nm in *pro*-2BTD. Nevertheless, the luminescence is bathochromically shifted in both when compared to the corresponding [2.2]PCP analogues. In addition, the luminescence in 2BTD displays a markedly stronger solvatochromism than *pro*-2BTD (Figure A4.8) or 1BTD studied by us previously,<sup>54</sup> which suggests an increased amount of charge-transfer character in the  $S_1 \rightarrow S_0$  transition, *i.e.*, a greater spatial extent of the  $S_1$  excitation.

The quantum yields of luminescence  $\phi_{\text{lum}}$  measured for  $\text{CH}_2\text{Cl}_2$  samples of *pro-2BTD* and **2BTD** are 0.82 and 0.22, respectively. While the  $\phi_{\text{lum}}$  determined for the macrocyclic precursors are comparable (Table 4.1), that of **2BTD** is approximately half of **2P** without BTD and reflects the narrowing of the HOMO–LUMO gap upon replacing one *para*-phenylene by a BTD unit. Yet, the measured  $\phi_{\text{lum}}$  value is respectable for a nanohoop fluorophore with such red-shifted luminescence.<sup>65–67</sup> Fit of the data of the excited state decay measured for the two compounds in  $\text{CHCl}_3$  using time-correlated single photon counting required two components with relatively similar amplitudes for both compounds ( $\sim 1.3$  and  $\sim 10$  ns), which most likely reflects the presence of two diastereomers dictated by the spatial orientation of the BTD unit with respect to the chiral [5]helicene unit (Figure A4.13).

Previously, we successfully resolved enantiomers of the macrocyclic precursor *pro-1BTD*, which allowed us, for the first time, to investigate chiroptical properties of such macrocycles.<sup>54</sup> We opted to use the same method in this work to resolve enantiomers of *pro-2BTD*. Although it allowed us to achieve excellent separation of the enantiomers (Figures A4.9), we were not successful in their subsequent isolation because the exposure of *pro-2BTD* to the chiral stationary phase and used eluent compromised its chemical stability and led to formation of the same product from each of *pro-2BTD* enantiomers during the HPLC experiments (Figures A4.10). We suspect that the presence of traces of acetic acid in the eluent are sufficient to induce decomposition of *pro-2BTD*, which we previously found stable in neat  $\text{CH}_2\text{Cl}_2$  or in the solid state. In addition, we made a curious observation after isolating an enantiomer, although as a mixture with the unknown product of rearrangement. HPLC analysis of such sample immediately after the enantiomer isolation revealed the presence of the other enantiomer in the mixture. This suggests that the racemization rate of *pro-2BTD* is markedly faster than that of *pro-1BTD*. Nevertheless, the process is slower than the observed *pro-2BTD* decomposition, which prevented us from investigating the kinetics to obtain the barrier.

To our delight, we successfully separated the enantiomers of **2BTD** with excellent purity using HPLC with identical chiral stationary phase and eluent  $\text{CH}_2\text{Cl}_2$ :*n*-heptane (1:1) as for *pro-2BTD* (Figures A4.9). The enantiomers are configurationally stable at room temperature, but we do observe racemization upon heating of the samples dissolved in toluene to 80 °C. We then analyzed the chiroptical properties of both **2BTD** enantiomers in  $\text{CH}_2\text{Cl}_2$  using ECD spectroscopy at room temperature.

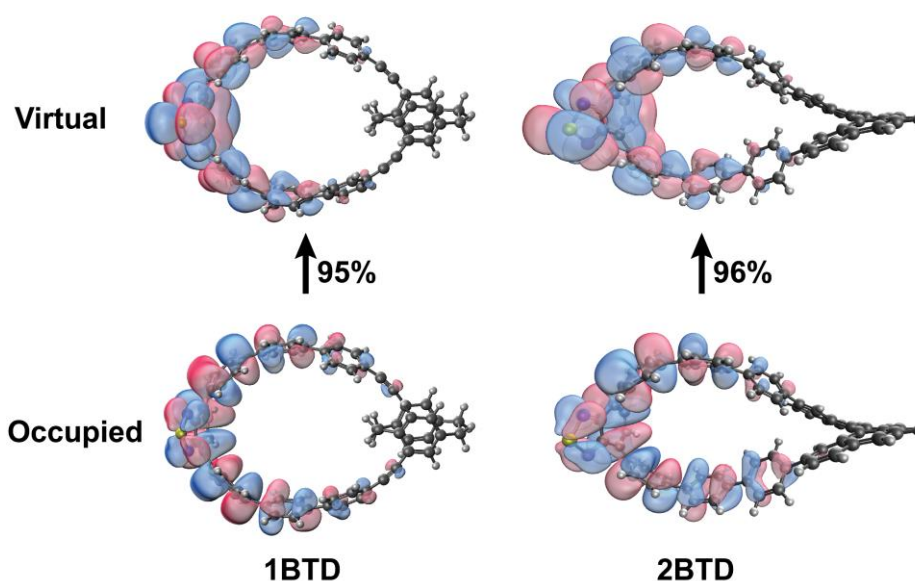


**Figure 4.3.** The natural transition orbitals (TD-CAM-B3LYP) for the  $S_0 \rightarrow S_1$  transition in **1BTD** and **2BTD**.

**Chiroptical properties and theoretical calculations:** The recorded ECD spectra with clear opposite Cotton effects (Figure 4.2, bottom) combined with our TD-DFT calculations permitted an unequivocal assignment of the configuration to each enantiomer. Unlike for the  $S_0 \rightarrow S_1$  transition ( $\sim 480$  nm), we observe high values of  $\Delta\epsilon$  for the excitation at the major absorption band ( $\sim 330$  nm). However, as mentioned in the Introduction, adjusting this type of chiroptical response for the overall absorption to obtain  $g_{abs}$  reveals that the dissymmetry is nearly equal through the entire spectrum.

**Table 4.1.** Summary of the photophysical properties.<sup>[a]</sup>

Compound	$\lambda_{abs}$ (nm) <sup>b</sup>	$\lambda_{em}$ (nm)	$\phi_{lum}$	$\epsilon$ <sup>[b]</sup> ( $10^4 \text{ M}^{-1} \text{ cm}^{-1}$ )	$ g_{abs} $ <sup>[c]</sup> ( $10^{-3}$ )	$ g_{lum} $ <sup>[c]</sup> ( $10^{-3}$ )	Stokes shift ( $\text{cm}^{-1}$ )
<b>1P</b>	<400, 328	470	0.72	– <sup>[h]</sup> , 3.95	$\sim 11$ <sup>[c]</sup> (20.1)	2.7 (2.3)	– <sup>[h]</sup>
<b>1BTD</b>	450, 324	609 (596 <sup>[d]</sup> )	0.48	0.3, 2.2	1.3 <sup>[c]</sup> (1.2)	0.5 (0.7)	5800
<i>pro</i> - <b>1BTD</b>	389, $\sim 320$	500 (473 <sup>[d]</sup> )	0.70	0.9, 3.5	0.3 <sup>[c]</sup> (0.22)	<0.1 (0.17)	5700
<b>2P</b>	$\sim 400$ , 340	498	0.46	0.8, 5.7	3.7 <sup>[c]</sup> (3.5)	1.0 (1.52)	4920
<b>2BTD</b>	479, 328	654	0.22	0.5, 7.3	1.8 <sup>[c]</sup> (1.2)	n.d. <sup>[i]</sup> (0.1)	5590
<i>pro</i> - <b>2BTD</b>	399, 288	526	0.82	0.5, 3.5	– <sup>[g]</sup> (0.7)	– <sup>[g]</sup> (0.35)	6050

<sup>[a]</sup> $\text{CH}_2\text{Cl}_2$  solutions at room temperature ( $\sim 10^{-6}$  M). <sup>[b]</sup>The values for the first and the second absorption maximum, respectively. <sup>[c]</sup>Maximum of  $g_{abs}$  for  $S_0 \rightarrow S_1$  transition. <sup>[d]</sup>At 420 nm for **2BTD**. <sup>[e]</sup>Estimated for the  $S_0 \rightarrow S_1$  transition from data in ref.<sup>44</sup> <sup>[f]</sup>TD-CAM-B3LYP/6-31g(d) values in parentheses. <sup>[g]</sup>Enantiomers could not be separated. <sup>[h]</sup>Cannot be determined because the  $S_0 \rightarrow S_1$  transition is not resolved. <sup>[i]</sup>Not determined.

The experimental  $g_{abs}$  for the two series of compounds (**1** and **2**; only theoretical  $g_{abs}$  for *pro*-**2BTD**) are summarized in Table 4.1 and offer a few observations to make. Firstly, the TD-DFT theoretical framework that we used in the current and previous works reproduce the experimental  $g_{abs}$  and also

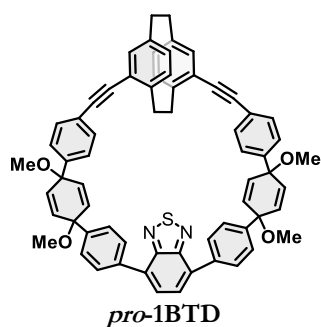
$g_{\mu m}$  values really well and provide credence for an in-dept analysis of experimental data and for predicting novel chiral compounds employing [2.2]PCP or helicenes using computational chemistry. The measurements and calculations show that forcing the exciton localization by using BTD instead of phenylene in series **2** compromises  $g_{abs}$  as we observed previously<sup>54</sup> in the series **1** with [2.2]PCP, but not to such a large extent. Nevertheless, **2P** or **2BTD** display inferior chiroptical response compared to **1P**, yet better than in **1BTD**. The full break in the conjugation in the precursor macrocycles clearly diminishes the chiroptical response, although theory predicts *pro*-**2BTD** to possess a little larger angle  $\theta$  between the  $\mu$  and  $m$  transition dipole moments (eq. 3, Table A4.4) and hence larger  $g_{abs}$ . Comparison of individual parameters according to eq. 3 in **1BTD** and **2BTD** (Tables A4.2–A4.6) reveals that the rotatory strength is enhanced in the former because of larger  $|\mu|$  and  $|m|$ . However, this enhancement is compensated in the final  $g_{abs}$  due to lower  $|\mu|$  in **2BTD**. The lower  $|m|$  by  $\sim 15\%$  in **2BTD** is due to absence of the ethynyl spacers, which decreases the inner area enclosed within the macrocycle compared to **1BTD**, in agreement with the observation of Uceda *et al.*<sup>52</sup> The values of angle  $\theta$  in both compounds are nearly identical, which suggests a similar extent of exciton delocalization in the two compounds. Combined with our observations from the steady-state spectroscopy, we argue that a more appreciable exciton delocalization using [5]helicene instead of *pseudo-meta* [2.2]PCP could not be achieved due to an insufficient orbital overlap between the segment of *para*-phenylenes and [5]helicene. The overlap is compromised by the relatively large dihedral angles between these units. For this reason, all the observed trends in (chir)optical properties are not strong. An ethynyl spacer, such as in compounds **1**, could mitigate this issue improving the exciton delocalization, which is now still mostly confined to the curved chromophore and responsible for somewhat similar  $g_{abs}$  in **2P** and **2BTD**. Yet,  $g_{abs}$  is nearly three times larger for **2P** in agreement with larger delocalization of the exciton into [5]helicene (compare NTOs in Figure A4.16). Therefore, alternation of *para*-phenylene and ethynyl units in chiral nanohoops could offer a strategy to avoid conformational perturbations due to steric hindrance. Finally, the use of [2.2]PCP with the *pseudo-para* connection appears as a more promising approach to achieve a strong chiroptical response in nanohoops with relatively low molecular symmetry than using [ $n$ ]carbohelicenes. However, configurational stability of such [2.2]PCP nanohoops must first be improved to permit resolution of enantiomers, possibly by a mechanical stabilization of the chirality as demonstrated previously by one of us.<sup>68</sup>

### 4.3 Conclusion

In summary, we synthesized two new macrocycles that incorporate [5]helicene as an axially chiral unit and a highly fluorescent benzothiadiazole group as a chromophore. The fully conjugated benzothiadiazole helicene carbon nano hoop displays significantly red-shifted fluorescence that extends well to the near-IR region with an appreciable luminescence quantum yield. Further steady-state spectroscopy investigation of the individual enantiomers of this compound allowed us to strengthen the hypothesis present in the literature that connects  $\pi$ -electron conjugation, exciton delocalization, and the achieved chiroptical response in the form of the electronic dissymmetry factor. Finally, the new experimental and theoretical data collated with the previous studies validate the remarkable accuracy of the used density functional theory method and opens opportunities to use it to explore the extensive chiral, macrocyclic compound space with large-scale computational approaches to find suitable candidates that display an exceptional electronic dissymmetry factor.

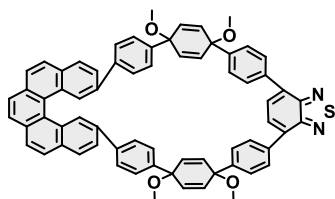
## 4.4 Appendix

**General remarks:** Additional material that can be found in the Supporting Information of the published paper (doi.org/10.1002/hlca.202400166) : General experimental details, variable-temperature (VT) NMR for *pro*-2BTD, Beer–Lambert plots, HPLC chromatograms and UV-vis and emission spectra of enantiopure (*P*) and (*M*)–2BTD, calculated CD spectra, NTOs, lifetime data, cartesian coordinates.



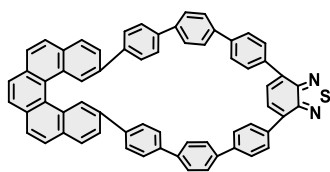
Compounds **6** were synthesized following the literature protocols.<sup>45</sup> Spectral data matched the values reported in the literature. Compound **7** is commercially available.

### Synthesis of *pro*-2BTD:



To a 250 ml round-bottom flask, **6** (100 mg, 0.090 mmol, 1 equiv), **7** (28 mg, 0.094 mmol, 1.05 equiv) and SPhos Pd Gen 3 (7 mg, 0.009 mmol, 0.1 equiv) were added. The flask was evacuated and backfilled with argon five times. 1,4-dioxane and 2 M aq K<sub>3</sub>PO<sub>4</sub> solution were sparged with Ar for 2 h prior to use. To the reaction mixture, dioxane (60 ml) was added and the solution was sparged with Ar for another 1 hour. The reaction mixture was heated to 80 °C at which point the degassed K<sub>3</sub>PO<sub>4</sub> solution (6 ml) was added dropwise. The reaction mixture was allowed to stir overnight at 80 °C. The solution was cooled down and filtered through celite and the flask was rinsed using dichloromethane. The filtrate was washed with brine, dried over sodium sulfate and volatiles were removed under reduced pressure. The product was purified first using silica gel chromatography (30% ethyl acetate in petroleum ether) and gel permeation chromatography (chloroform) to afford the product *pro*-2BTD as a green crystalline solid (50 mg, 56%). **<sup>1</sup>H NMR** (500 MHz, CDCl<sub>3</sub>, 298 K, δ/ppm) δ 8.22 (d, J = 1.8 Hz, 2H), 7.84 (m, 8H), 7.76 (d, J = 8.6 Hz, 2H), 7.74 (s, 2H), 7.70 (s, 2H), 7.49 (d, J = 8.6 Hz, 4H), 7.31 (dd, J = 8.5, 1.8 Hz, 2H), 7.08 (d, J = 8.5, 4H), 6.98 (d, J = 8.5 Hz, 4H), 6.37 (dd, J = 10.4, 2.4 Hz, 2H), 6.21 (dd, J = 10.3, 2.5 Hz, 2H), 6.12 (dd, J = 10.2, 2.5 Hz, 2H), 5.87 (dd, J = 10.2, 2.5 Hz, 2H), 3.49 (s, 6H), 3.26 (s, 6H). **<sup>13</sup>C NMR** (126 MHz, CDCl<sub>3</sub>, 298 K, δ/ppm) δ 154.53, 142.83, 141.68, 140.79, 138.30, 137.31, 134.97, 134.40, 133.05, 132.97, 132.63, 131.81, 131.67, 131.34, 129.55, 129.12, 128.00, 127.82, 127.60, 127.43, 127.05, 126.52, 126.05, 125.32, 77.42, 77.37, 77.16, 76.91, 75.44, 74.48, 52.54, 51.65. **HRMS** (FD+): *m/z* calculated for C<sub>68</sub>H<sub>50</sub>N<sub>2</sub>O<sub>4</sub>S: 990.3491, found 990.3484.

## Synthesis of 2BTD:



An  $\text{H}_2\text{SnCl}_4$  solution was freshly prepared:  $\text{SnCl}_2 \cdot 2\text{H}_2\text{O}$  (147 mg, 138  $\mu\text{mol}$ ) was suspended in THF (2.5 mL) and 37% aqueous HCl (100  $\mu\text{L}$ ) was added, and the resulting mixture was degassed while stirring for 30 min. To a 25 ml round bottom flask, *pro-2BTD* (40 mg, 0.040 mmol, 1 equiv) was dissolved in 5 ml THF and  $\text{H}_2\text{SnCl}_4$  solution (1.5 ml, 0.36 mmol, 0.241 M, 9 equiv) was added dropwise. The fluorescence of the solution immediately changes from bright green to orange red. After completion of the reaction, the reaction mixture was quenched with 2M aqueous NaOH solution. The aqueous layer was extracted with dichloromethane and organic layers were combined and dried over sodium sulfate. The crude mixture was purified by column chromatography ( $\text{SiO}_2$ , 100% toluene) followed by gel permeation chromatography (chloroform) affording a **2BTD** as a red solid (15 mg, 43%). The nanohoop shows slow decomposition overtime at ambient temperature.  **$^1\text{H}$  NMR**:  $^1\text{H}$  NMR (500 MHz,  $\text{CDCl}_3$ , 298 K,  $\delta/\text{ppm}$ ): 8.97 (d,  $J = 11.6$  Hz, 2H), 8.06 (m, 2H), 7.96 (d,  $J = 8.5$  Hz, 2H), 7.87 (d,  $J = 8.9$  Hz, 4H), 7.73 (d,  $J = 8.4$  Hz, 2H), 7.66 (d,  $J = 8.4$  Hz, 2H), 7.55 (d,  $J = 8.5$  Hz, 2H), 7.52–7.42 (m, 10H), 7.41–7.29 (m, 12H), 1.56, 1.26, 0.86.  **$^{13}\text{C}$  NMR** (126 MHz,  $\text{CDCl}_3$ , 298 K,  $\delta/\text{ppm}$ ):  $\delta$  155.34, 155.11, 140.34, 140.05, 138.55, 138.54, 138.33, 138.25, 137.99, 137.67, 137.66, 137.49, 137.17, 137.10, 136.19, 133.32, 132.72, 132.71, 132.05, 132.03, 131.58, 131.48, 131.46, 130.72, 129.51, 128.92, 128.11, 127.92, 127.49, 127.43, 127.37, 127.29, 127.21, 127.12, 127.06, 126.85, 126.83, 126.79, 126.54, 126.40, 125.38, 125.31. (A good carbon spectrum was not obtained due to poor solubility of nanohoop in most organic solvents). The target nanohoop is poorly soluble in deuterated chloroform, therefore, only the chemical shifts fully visible are reported here). **HRMS (MALDI+)**: calculated for  $\text{C}_{64}\text{H}_{38}\text{N}_2\text{S}$ : 866.2755, found 866.2340.

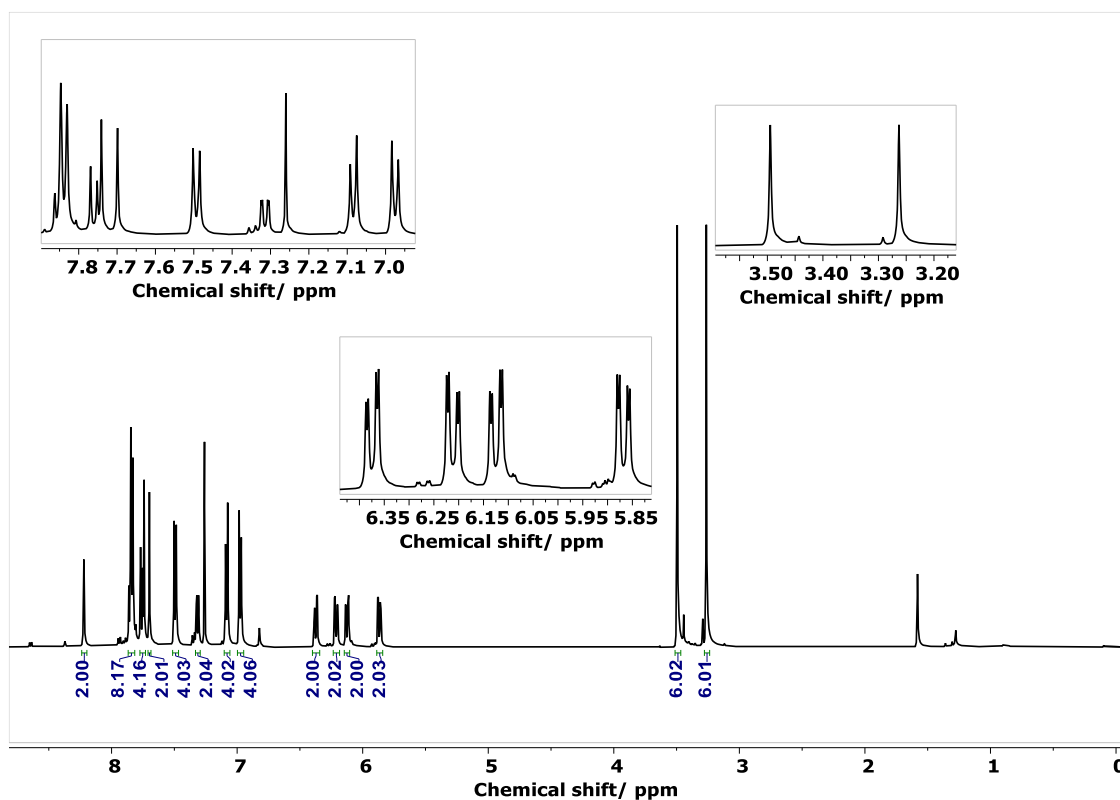
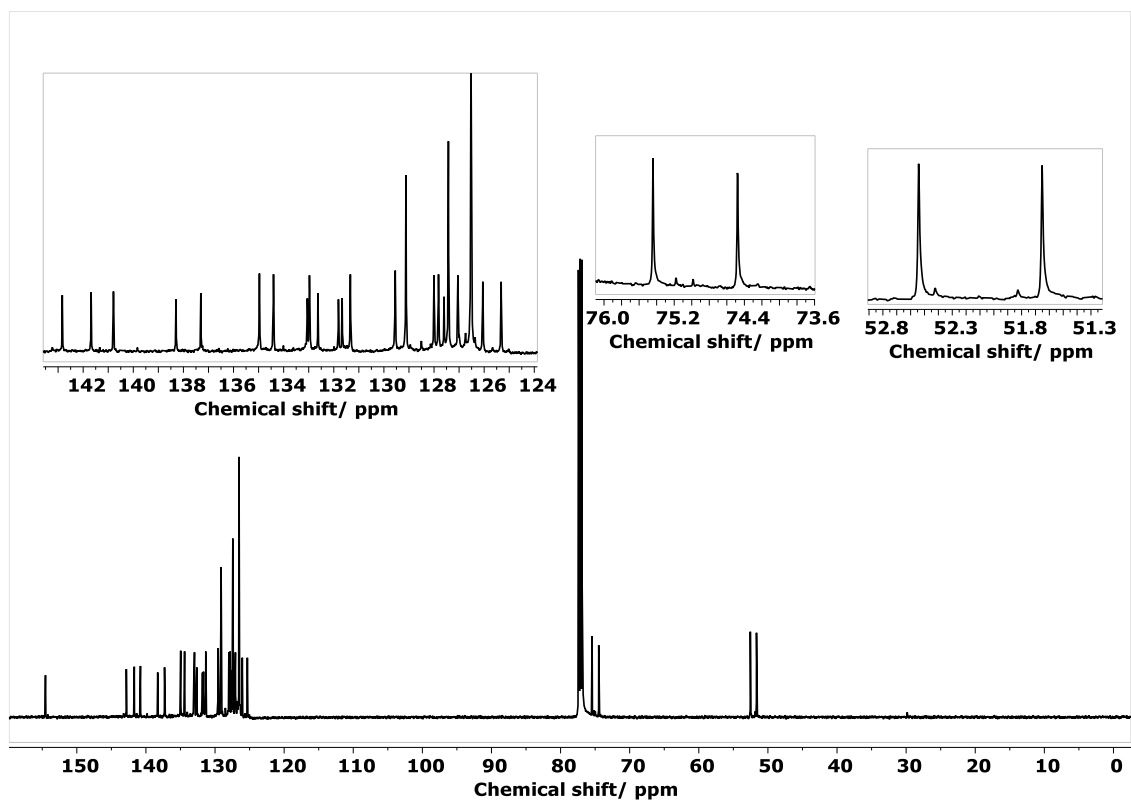
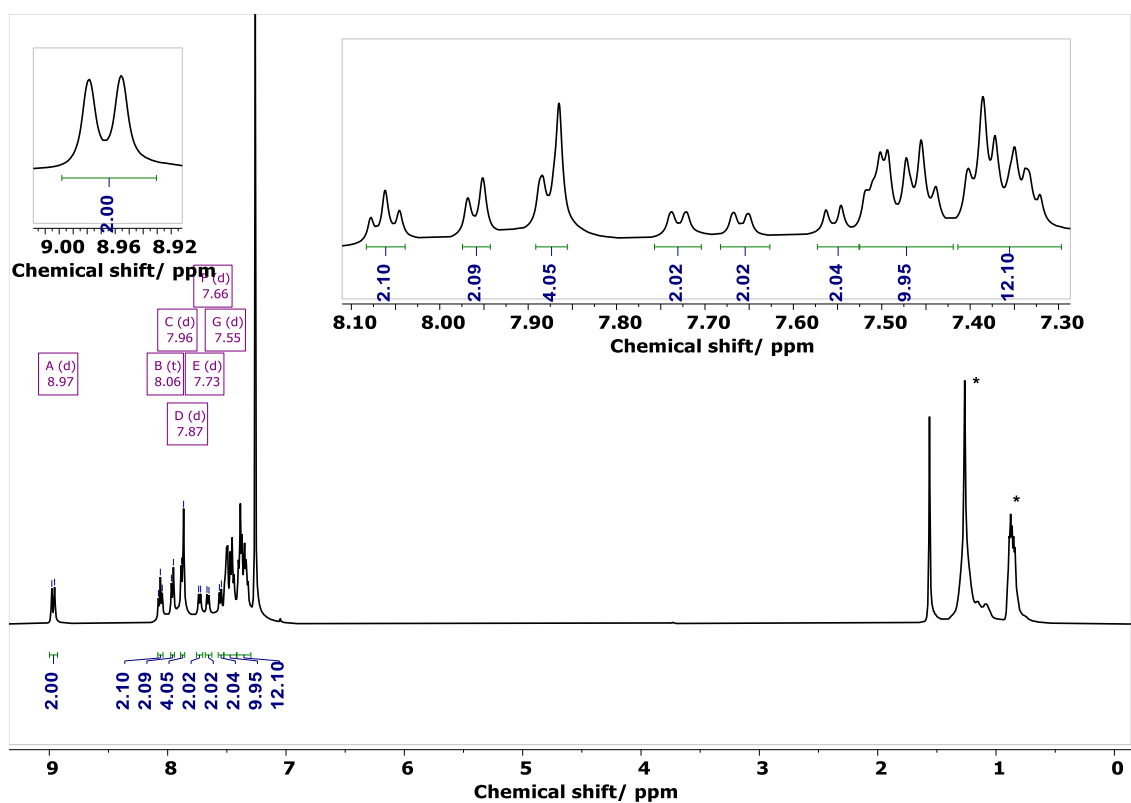


Figure A4.1.  $^1\text{H}$  NMR spectrum of compound *pro-2BTD* in  $\text{CDCl}_3$ .

Figure A4.2.  $^{13}\text{C}$  NMR spectrum of compound *pro*-2BTD in  $\text{CDCl}_3$ .Figure A4.3.  $^1\text{H}$  NMR spectrum of compound 2BTD in  $\text{CDCl}_3$ . \* = grease

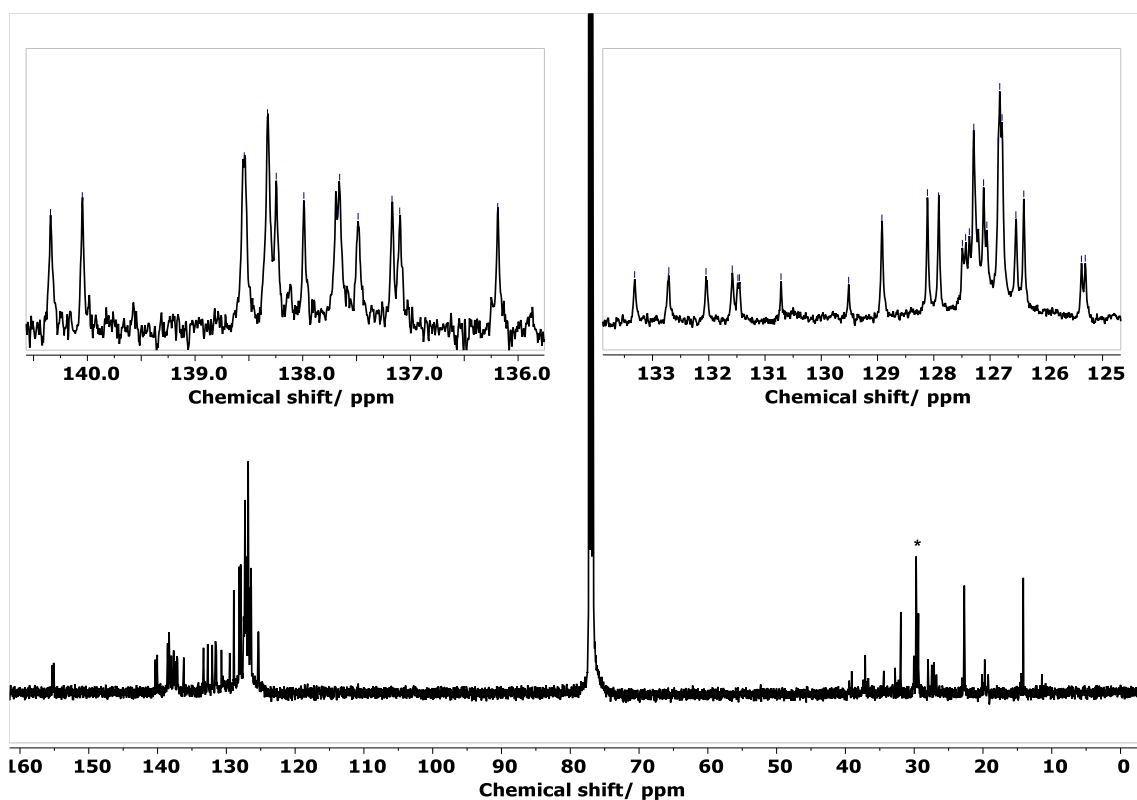


Figure A4.4.  $^{13}\text{C}$  NMR spectrum of compound 2BTD in  $\text{CDCl}_3$ . \* = grease (10 – 40 ppm)

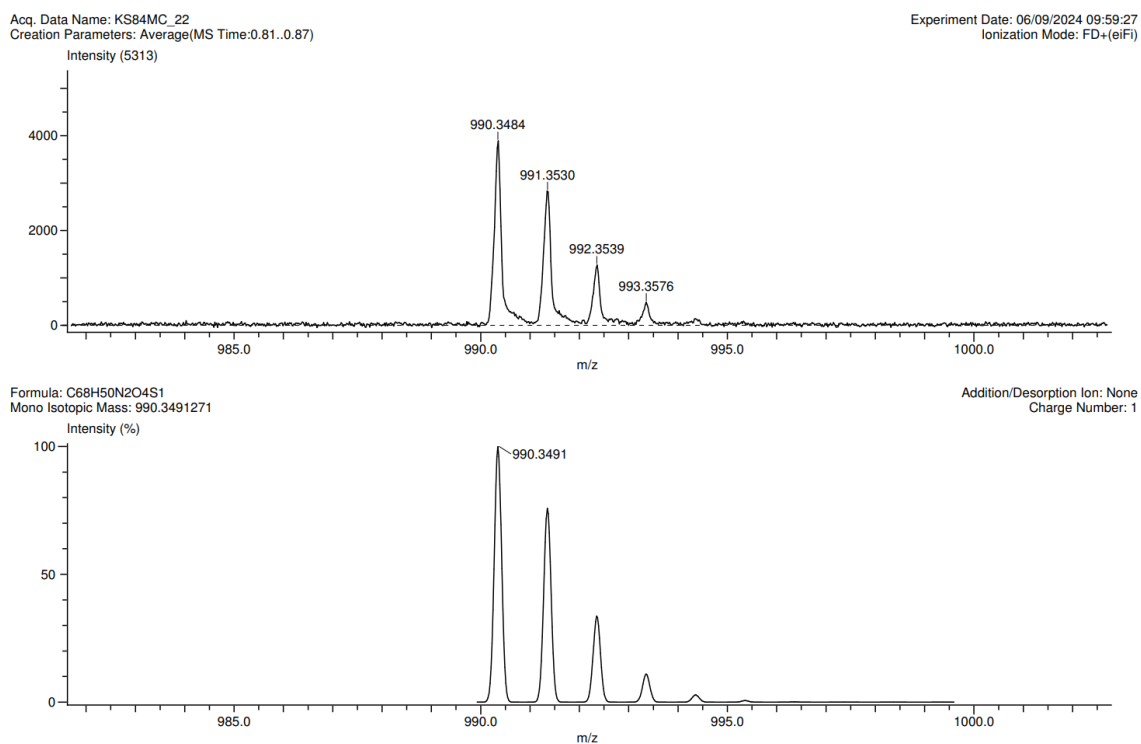


Figure A4.5. HRMS for compound *pro*-2BTD.

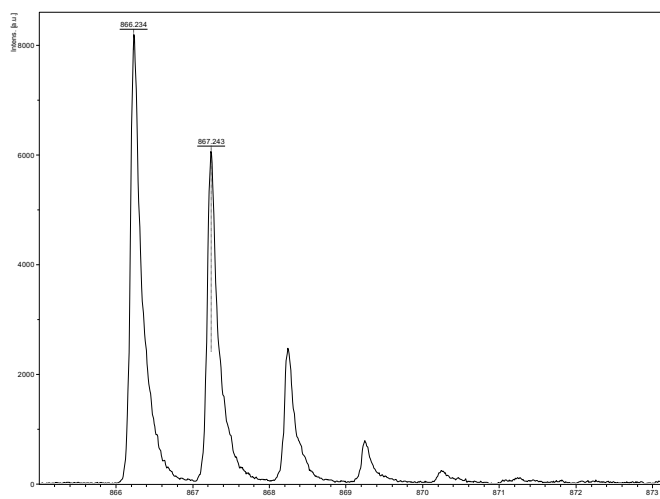


Figure A4.6. HRMS for compound **2BTD**.

**Photophysical Properties:** We measured the photophysical properties of *pro*-**2BTD** and **2BTD**. Enantiopure (*M*)-**2BTD** was used for all spectroscopic measurements (see below). Excitation wavelength for all fluorescence measurements was 350 nm unless stated otherwise.

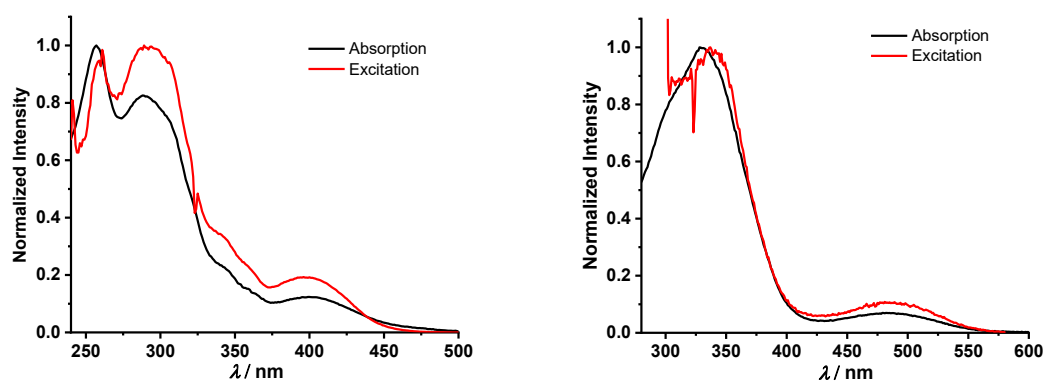


Figure A4.7. Optical purity check of *pro*-**2BTD** (left) and **2BTD** (right) in dichloromethane.

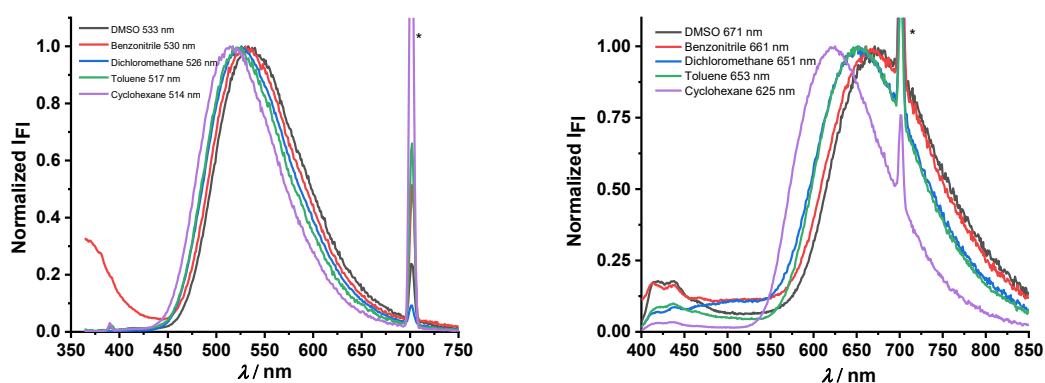
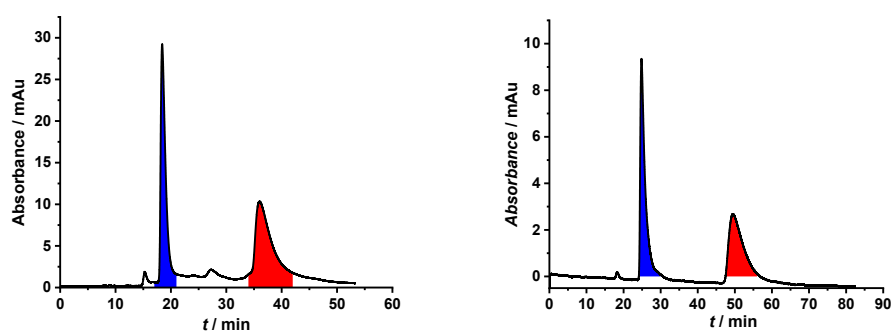


Figure A4.8. Emission spectra of *pro*-**2BTD** (left) and **2BTD** (right) in different solvents with emission maxima reported in the legend of the figure. \* = scattered light.

**Luminescence quantum yield measurements:** Absolute quantum yield of *pro*-2BTD (0.82) and 2BTD (0.22) was measured in dichloromethane using an integrating sphere setup. Absorbance of the samples at excitation wavelength (350 nm for *pro*-2BTD and 360 nm for 2BTD) was 0.1.

**Chiral HPLC:** Enantiomers of *pro*-2BTD and 2BTD were resolved on a preparative scale using recycling HPLC equipped with a Chiralpak IG (20x250mm) column by Daicel. For both compounds, 50% DCM in *n*-heptane was used as an eluent at 10 mL min<sup>-1</sup> flow rate. The enantiomers of 2BTD were individually injected on analytical HPLC equipped with a Chiralpak IG (4.6x250mm) to check the purity of the samples and possible racemization behaviour. Further, UV-vis absorption and emission spectra was also measured for the respective enantiomers of 2BTD. The enantiomers of *pro*-2BTD were also separated and collected in a similar manner. However, the decomposition of the enantiomers was observed after elution from the column. The enantiomers were injected on analytical HPLC to check the purity. A new peak corresponding to the decomposition product (RT:20min) was visible in both the enantiomer chromatograms. \* in all HPLC chromatograms denotes a change in the signal baseline due to the instability of the UV detector. 2BTD racemizes at elevated temperatures but is configurationally sufficiently stable at room temperature.



**Figure A4.9.** HPLC chromatogram of *pro*-2BTD and 2BTD on the semi-prep recycling HPLC. A racemate was injected and enantiomer 1 (blue) and enantiomer 2 (red) were collected and correspond to (*P*)- and (*M*)- enantiomers, respectively, using 50-50 DCM-*n*-heptane as eluent and flow rate of 10 ml/min.

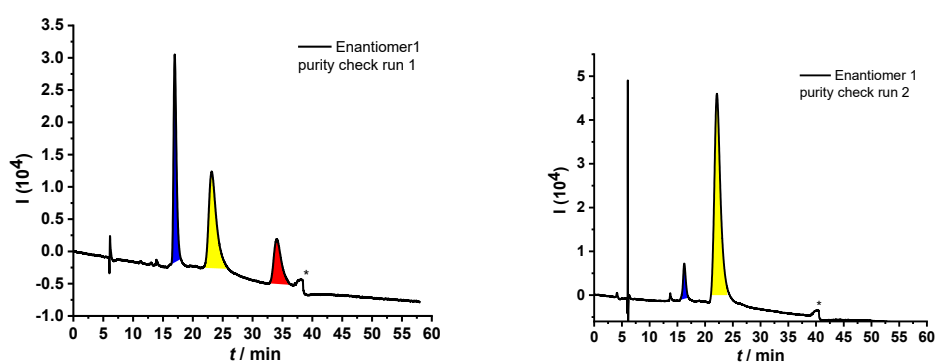


**Figure A4.10.** HPLC chromatogram of Enantiomer 1 of *pro*-2BTD on the analytical HPLC right after the separation (left) and two days after the separation (right) on semi-prep column. Decomposition product (RT: 20min) colored in yellow. \*a change in the signal baseline due to the instability of the UV detector. Conditions: 50-50 DCM-*n*-heptane as an eluent and flow rate of 0.5 ml/min for purity check (RT:16 min). Similar behaviour was observed for enantiomer 2.

**Chiroptical Properties:** Circular dichroism (CD) spectra of **2BTD** were measured in dichloromethane. First, samples of enantiomers of similar concentrations ( $\sim 11 \mu\text{M}$ ) were prepared and their absorbance spectra was recorded.

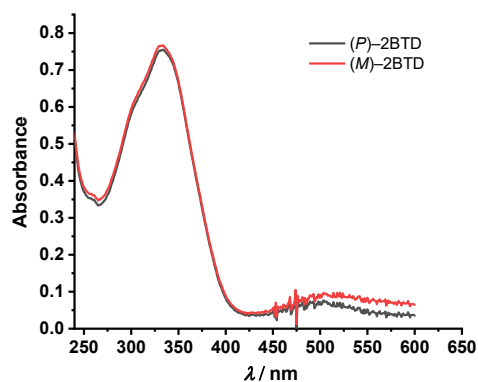


Figure A4.11. UV-vis absorption spectra of enantiomers (*P*)- and (*M*)- of **2BTD** in dichloromethane.

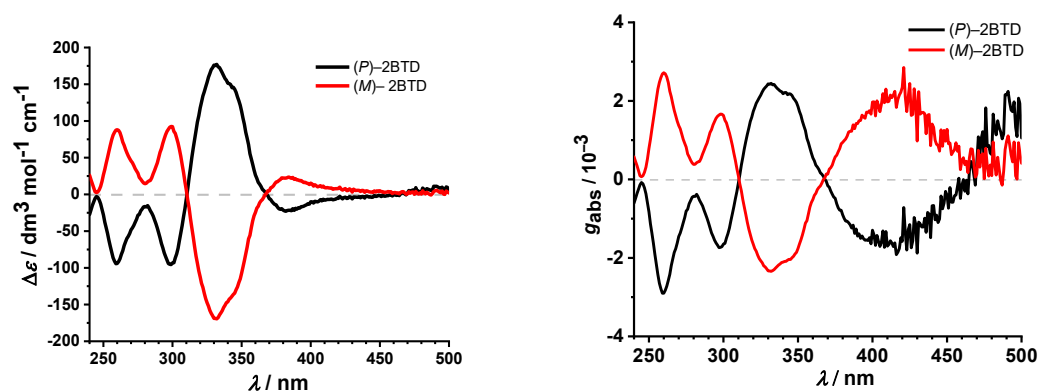


Figure A4.12. CD spectra of enantiomers of **2BTD** (left) and plot of  $g_{\text{abs}}$  of individual **2BTD** enantiomers (right).

**DFT Calculations:** Calculations were performed with Gaussian 16<sup>69</sup> (release C.02) software. The ground state geometries were optimized at D3-B3LYP/6-31g(d) level of theory. The character of found stationary points was confirmed by a subsequent frequency calculation. Default integration grid (UltraFine) was used in all calculations.

**Conformers of NanoHoop:** Two conformers of **2BTD** were found. They differ in the orientation of the BTD moiety relative to the cavity (Figure A4.13). The results are consistent with each other for both conformers and are reported only for conformer B as the lowest energy conformer for the sake of clarity.

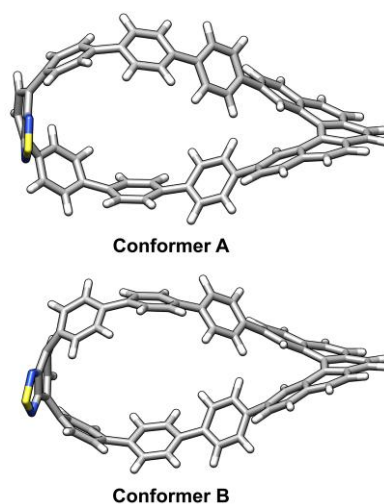


Figure A4.13. Geometries of lowest energy conformers of 2BTD.

Table A4.1. Relative Gibbs energies and Boltzmann distribution at 298 K of two main conformers of 2BTD.

Conformer	$\Delta G_r / \text{kcal mol}^{-1}$	$x / \%$
A	1.06	14.4
B	0	85.6

**TD-DFT:** CAM-B3LYP/6-31g(d) was used for all TD-DFT calculations. Geometries of the 1st excited states were optimized at the same level of theory.

Table A4.2. Calculated energies ( $E$ ), oscillator strengths ( $f$ ), electric ( $\mu$ ) and magnetic ( $m$ ) transition dipole moments, and angles ( $\theta$ ) between them, rotatory strengths ( $R$ , velocity form), dipole strengths ( $D$ ) and calculated dissymmetry factor ( $g_{abs}$ ) values for respective transitions of (P)-2BTD-conformer A.

Transition	$E / \text{eV}$	$\lambda / \text{nm}$	$f$	$ \mu  / 10^{-18} \text{ esu} \cdot \text{cm}$	$ m  / 10^{-20} \text{ erg} \cdot \text{G}^{-1}$	$\theta / ^\circ$	$R / 10^{-40} \text{ esu erg cm G}^{-1}$	$D / 10^{-36} \text{ esu}^2 \text{ cm}^2 \text{ erg}^2 \text{ G}^{-2}$	$g_{abs} / 10^{-3}$
$S_0 \rightarrow S_1$	2.66	466	0.2424	4.90	5.03	89.89	4.9	24.04	0.08
$S_0 \rightarrow S_2$	3.67	337	0.0007	0.22	0.20	86.29	0.3	0.05	2.25
$S_0 \rightarrow S_3$	3.73	332	0.9673	8.26	1.84	103.71	-357.7	68.30	-2.09
$S_0 \rightarrow S_4$	3.80	326	0.1058	2.71	5.93	86.8	90.4	7.34	4.92

Table A4.3. Calculated energies ( $E$ ), oscillator strengths ( $f$ ), electric ( $\mu$ ) and magnetic ( $m$ ) transition dipole moments, and angles ( $\theta$ ) between them, rotatory strengths ( $R$ , velocity form), dipole strengths ( $D$ ) and calculated dissymmetry factor ( $g_{abs}$ ) values for respective transitions of (P)-2BTD-conformer B.

Transition	$E / \text{eV}$	$\lambda / \text{nm}$	$f$	$ \mu  / 10^{-18} \text{ esu} \cdot \text{cm}$	$ m  / 10^{-20} \text{ erg} \cdot \text{G}^{-1}$	$\theta / ^\circ$	$R / 10^{-40} \text{ esu erg cm G}^{-1}$	$D / 10^{-36} \text{ esu}^2 \text{ cm}^2 \text{ erg}^2 \text{ G}^{-2}$	$g_{abs} / 10^{-3}$
$S_0 \rightarrow S_1$	2.76	449	0.2503	4.89	5.09	91.63	-72.4	23.91	-1.21
$S_0 \rightarrow S_2$	3.67	337	0.0003	0.16	0.22	95.5	-0.3	0.03	-5.07
$S_0 \rightarrow S_3$	3.77	329	0.1124	2.80	6.34	94.55	-139.5	7.87	-7.09
$S_0 \rightarrow S_4$	3.83	323	1.0785	8.61	1.85	106.08	-434.1	74.20	-2.34

**Table A4.4.** Calculated energies ( $E$ ), oscillator strengths ( $f$ ), electric ( $\mu$ ) and magnetic ( $m$ ) transition dipole moments, and angles ( $\theta$ ) between them, rotatory strengths ( $R$ , velocity form), dipole strengths ( $D$ ) and calculated dissymmetry factor ( $g_{abs}$ ) values for respective transitions of (*P*)-*pro*-2BTD.

Transition	$E / \text{eV}$	$\lambda / \text{nm}$	$f$	$ \mu  / 10^{-18} \text{ esu} \cdot \text{cm}$	$ m  / 10^{-20} \text{ erg} \cdot \text{G}^{-1}$	$\theta / ^\circ$	$R / 10^{-40} \text{ esu erg cm G}^{-1}$	$D / 10^{-36} \text{ esu}^2 \text{ cm}^2 \text{ erg}^2 \text{ G}^{-2}$	$g_{abs} / 10^{-3}$
$S_0 \rightarrow S_1$	3.24	383	0.2789	4.77	2.86	91.54	-37.3	22.73	-0.66
$S_0 \rightarrow S_2$	3.67	338	0.0012	0.30	0.09	105.85	-0.8	0.09	-3.58
$S_0 \rightarrow S_3$	3.85	322	0.1672	3.38	2.96	54.78	578.7	11.46	20.21
$S_0 \rightarrow S_4$	3.98	312	0.0055	0.60	0.15	95	-0.8	0.36	-0.89

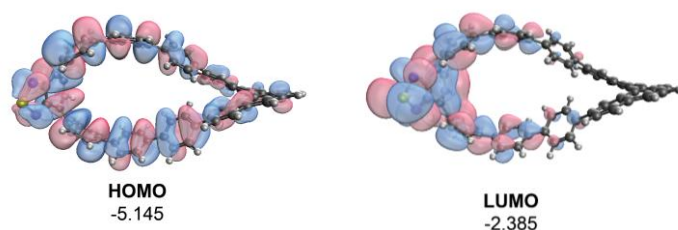
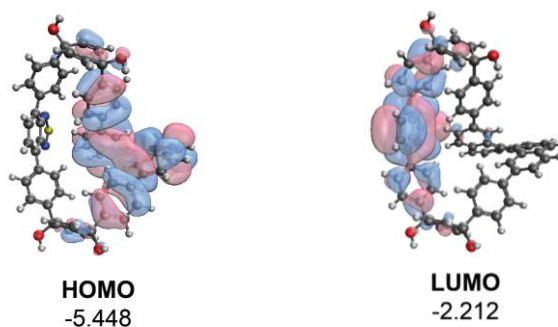
**Table A4.5.** Calculated energies ( $E$ ), oscillator strengths ( $f$ ), electric ( $\mu$ ) and magnetic ( $m$ ) transition dipole moments, and angles ( $\theta$ ) between them, rotatory strengths ( $R$ , velocity form), dipole strengths ( $D$ ) and calculated dissymmetry factor ( $g_{lum}$ ) values for  $S_1 \rightarrow S_0$  transitions of (*P*)-enantiomers of respective compounds.

Compound	$E / \text{eV}$	$\lambda / \text{nm}$	$f$	$ \mu  / 10^{-18} \text{ esu} \cdot \text{cm}$	$ m  / 10^{-20} \text{ erg} \cdot \text{G}^{-1}$	$\theta / ^\circ$	$R / 10^{-40} \text{ esu erg cm G}^{-1}$	$D / 10^{-36} \text{ esu}^2 \text{ cm}^2 \text{ erg}^2 \text{ G}^{-2}$	$g_{lum} / 10^{-3}$
2BTD-confA	1.87	664	0.2508	5.95	3.95	89.44	24.2	35.42	0.27
2BTD-confB	1.92	645	0.2677	6.07	4.20	89.81	8.6	36.84	0.09
<i>pro</i> -2BTD	2.43	511	0.3326	6.01	2.89	91.00	-31.6	36.14	-0.35

**Table A4.6.** Calculated energies ( $E$ ), oscillator strengths ( $f$ ), electric ( $\mu$ ) and magnetic ( $m$ ) transition dipole moments, and angles ( $\theta$ ) between them, rotatory strengths ( $R$ , velocity form), dipole strengths ( $D$ ) and calculated dissymmetry factor ( $g_{lum}$ ) values for  $S_0 \rightarrow S_1$  transitions of (*P*)-enantiomers of respective compounds. Data taken from Kovida *et al.*<sup>54</sup>

Compound	$E / \text{eV}$	$f$	$ \mu  / 10^{-18} \text{ esu} \cdot \text{cm}$	$ m  / 10^{-20} \text{ erg} \cdot \text{G}^{-1}$	$\theta / ^\circ$	$R / 10^{-40} \text{ esu erg cm G}^{-1}$	$D / 10^{-36} \text{ esu}^2 \text{ cm}^2 \text{ erg}^2 \text{ G}^{-2}$	$g_{abs} / 10^{-3}$
1BTD	2.9181	0.3393	5.54	5.78	91.69	-95.6253	30.66	-1.25
<i>pro</i> -1BTD	3.3321	0.3268	5.09	3.69	90.44	-14.3600	25.87	-0.22

## Frontier molecular orbitals

Figure A4.14. Frontier molecular orbitals and their energies in eV for **2BTD**.Figure A4.15. Frontier molecular orbitals and their energies in eV for *pro*-**2BTD**.

**Transitions Investigation:** The first 10 transitions were investigated. Natural transition orbitals were printed for first 4 transitions in nanoHoop to make a clearer picture about the transitions.

Table A4.7. TD-DFT data of first 4 transitions in **2BTD**–conformer B.

Transition	$E / \text{eV}$	$\lambda / \text{nm}$	$f$	Orbital contributions <sup>a</sup>
$S_0 \rightarrow S_1$	2.76	449	0.2503	HOMO $\rightarrow$ LUMO (87%)
$S_0 \rightarrow S_2$	3.67	337	0.0003	HOMO-2 $\rightarrow$ LUMO+1 (26%) HOMO-1 $\rightarrow$ LUMO+3 (39%)
$S_0 \rightarrow S_3$	3.77	329	0.1124	HOMO-1 $\rightarrow$ LUMO+1 (35%) HOMO $\rightarrow$ LUMO+2 (32%)
$S_0 \rightarrow S_4$	3.83	323	1.0785	HOMO-3 $\rightarrow$ LUMO (39%) HOMO-1 $\rightarrow$ LUMO (31%)

<sup>a</sup>Only the contributions larger than 10% or the highest contributing transitions are listed.

Table A4.8. TD-DFT data of first 4 transitions in *pro*-**2BTD**.

Transition	$E / \text{eV}$	$\lambda / \text{nm}$	$f$	Orbital contributions <sup>a</sup>
$S_0 \rightarrow S_1$	3.24	383	0.2789	HOMO-1 $\rightarrow$ LUMO (92%)
$S_0 \rightarrow S_2$	3.67	338	0.0012	HOMO-2 $\rightarrow$ LUMO (33%) HOMO $\rightarrow$ LUMO+1 (52%)
$S_0 \rightarrow S_3$	3.85	322	0.1672	HOMO $\rightarrow$ LUMO+1 (75%)
$S_0 \rightarrow S_4$	3.98	312	0.0055	HOMO-3 $\rightarrow$ LUMO (13%) HOMO $\rightarrow$ LUMO (75%)

<sup>a</sup>Only the contributions larger than 10% or the highest contributing transitions are listed.

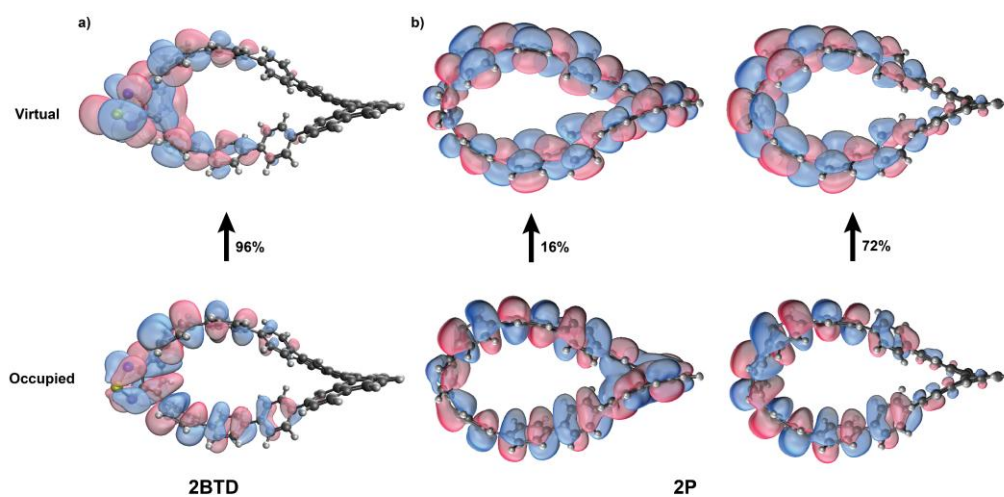


Figure A4.16. Natural transition orbitals of  $S_0 \rightarrow S_1$  transition in a) 2BTD b) 2P.

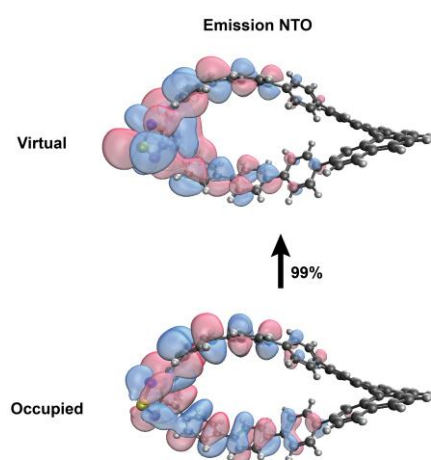


Figure A4.17. Natural transition orbitals of  $S_1 \rightarrow S_0$  transition (right) in 2BTD.

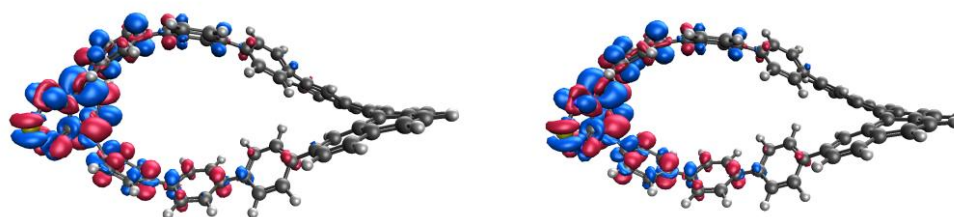


Figure A4.18. Transition density of  $S_0 \rightarrow S_1$  transition (left) and  $S_1 \rightarrow S_0$  transition (right) in 2BTD.

## 4.5 References

- (1) Rickhaus, M.; Mayor, M.; Juriček, M. Strain-Induced Helical Chirality in Polyaromatic Systems. *Chem. Soc. Rev.* **2016**, *45* (6), 1542–1556. <https://doi.org/10.1039/C5CS00620A>.
- (2) Rickhaus, M.; Mayor, M.; Juriček, M. Chirality in Curved Polyaromatic Systems. *Chem. Soc. Rev.* **2017**, *46* (6), 1643–1660. <https://doi.org/10.1039/C6CS00623J>.
- (3) Weiland, K. J.; Gallego, A.; Mayor, M. Beyond Simple Substitution Patterns – Symmetrically Tetrasubstituted [2.2]Paracyclophanes as 3D Functional Materials. *Eur. J. Org. Chem.* **2019**, *2019* (20), 3073–3085. <https://doi.org/10.1002/ejoc.201900061>.
- (4) Barron, L. D. Symmetry and Chirality: Where Physics Shakes Hands with Chemistry and Biology. *Isr. J. Chem.* **2021**, *61* (9–10), 517–529. <https://doi.org/10.1002/ijch.202100044>.
- (5) Meyer-Ilse, J.; Akimov, D.; Dietzek, B. Recent Advances in Ultrafast Time-Resolved Chirality Measurements: Perspective and Outlook. *Laser Photonics Rev.* **2013**, *7* (4), 495–505. <https://doi.org/10.1002/lpor.201200065>.
- (6) Brandt, J. R.; Salerno, F.; Fuchter, M. J. The Added Value of Small-Molecule Chirality in Technological Applications. *Nat. Rev. Chem.* **2017**, *1* (6), 1–12. <https://doi.org/10.1038/s41570-017-0045>.
- (7) Kuznetsova, V.; Gromova, Y.; Martinez-Carmona, M.; Purcell-Milton, F.; Ushakova, E.; Cherevko, S.; Maslov, V.; Gun'ko, Y. K. Ligand-Induced Chirality and Optical Activity in Semiconductor Nanocrystals: Theory and Applications. *Nanophotonics* **2021**, *10* (2), 797–824. <https://doi.org/10.1515/nanoph-2020-0473>.
- (8) Lininger, A.; Palermo, G.; Guglielmelli, A.; Nicoletta, G.; Goel, M.; Hinczewski, M.; Strangi, G. Chirality in Light–Matter Interaction. *Adv. Mater.* **2023**, *35* (34), 2107325. <https://doi.org/10.1002/adma.202107325>.
- (9) Naaman, R. Chirality – Beyond the Structural Effects. *Isr. J. Chem.* **2016**, *56* (11–12), 1010–1015. <https://doi.org/10.1002/ijch.201600102>.
- (10) Evers, F.; Aharony, A.; Bar-Gill, N.; Entin-Wohlman, O.; Hedegård, P.; Hod, O.; Jelinek, P.; Kamieniarz, G.; Lemeshko, M.; Michaeli, K.; Mujica, V.; Naaman, R.; Paltiel, Y.; Refaely-Abramson, S.; Tal, O.; Thijssen, J.; Thoss, M.; van Ruitenbeek, J. M.; Venkataraman, L.; Waldeck, D. H.; Yan, B.; Kronik, L. Theory of Chirality Induced Spin Selectivity: Progress and Challenges. *Adv. Mater.* **2022**, *34* (13), 2106629. <https://doi.org/10.1002/adma.202106629>.
- (11) Han, J.; Guo, S.; Lu, H.; Liu, S.; Zhao, Q.; Huang, W. Recent Progress on Circularly Polarized Luminescent Materials for Organic Optoelectronic Devices. *Adv. Opt. Mater.* **2018**, *6* (17), 1800538. <https://doi.org/10.1002/adom.201800538>.
- (12) Niu, X.; Zhao, R.; Yan, S.; Pang, Z.; Li, H.; Yang, X.; Wang, K. Chiral Materials: Progress, Applications, and Prospects. *Small* **2023**, *19* (38), 2303059. <https://doi.org/10.1002/smll.202303059>.
- (13) Guo, L.; Hu, S.; Gu, X.; Zhang, R.; Wang, K.; Yan, W.; Sun, X. Emerging Spintronic Materials and Functionalities. *Adv. Mater.* **2024**, *36* (22), 2301854. <https://doi.org/10.1002/adma.202301854>.
- (14) Warnke, I.; Furche, F. Circular Dichroism: Electronic. *WIREs Comput. Mol. Sci.* **2012**, *2* (1), 150–166. <https://doi.org/10.1002/wcms.55>.
- (15) Aranda, D.; Schuster, N. J.; Xiao, X.; Ávila Ferrer, F. J.; Santoro, F.; Nuckolls, C. Origin of Chiroptic Amplification in Perylene-Diimide Helicenes. *J. Phys. Chem. C* **2021**, *125* (4), 2554–2564. <https://doi.org/10.1021/acs.jpcc.0c11382>.
- (16) Bao, S. T.; Jiang, H.; Jin, Z.; Nuckolls, C. Fusing Perylene Diimide with Helicenes. *Chirality* **2023**, *35* (10), 656–672. <https://doi.org/10.1002/chir.23561>.
- (17) Nagata, Y.; Mori, T. Irreverent Nature of Dissymmetry Factor and Quantum Yield in Circularly Polarized Luminescence of Small Organic Molecules. *Front. Chem.* **2020**, *8*.
- (18) Covington, C. L.; Polavarapu, P. L. Solvation Dependence Observed in the Electronic Dissymmetry Factor Spectra: How Much Information Are We Missing by Analyzing the Circular Dichroism Spectra Alone? *Phys. Chem. Chem. Phys.* **2016**, *18* (20), 13912–13917. <https://doi.org/10.1039/C6CP01247G>.
- (19) Gon, M.; Morisaki, Y.; Chujo, Y. Optically Active Phenylethene Dimers Based on Planar Chiral Tetrasubstituted [2.2]Paracyclophane. *Chem. – Eur. J.* **2017**, *23* (26), 6323–6329. <https://doi.org/10.1002/chem.201605598>.
- (20) Hassan, Z.; Spuling, E.; Knoll, D. M.; Lahann, J.; Bräse, S. Planar Chiral [2.2]Paracyclophanes: From Synthetic Curiosity to Applications in Asymmetric Synthesis and Materials. *Chem. Soc. Rev.* **2018**, *47* (18), 6947–6963. <https://doi.org/10.1039/C7CS00803A>.
- (21) Liao, C.; Zhang, Y.; Ye, S.-H.; Zheng, W.-H. Planar Chiral [2.2]Paracyclophane-Based Thermally Activated Delayed Fluorescent Materials for Circularly Polarized Electroluminescence. *ACS Appl. Mater. Interfaces* **2021**, *13* (21), 25186–25192. <https://doi.org/10.1021/acsami.1c04779>.
- (22) Shen, Y.; Chen, C.-F. Helicenes: Synthesis and Applications. *Chem. Rev.* **2012**, *112* (3), 1463–1535. <https://doi.org/10.1021/cr200087r>.
- (23) Zhao, W.-L.; Li, M.; Lu, H.-Y.; Chen, C.-F. Advances in Helicene Derivatives with Circularly Polarized Luminescence. *Chem. Commun.* **2019**, *55* (92), 13793–13803. <https://doi.org/10.1039/C9CC06861A>.

- (24) Cei, M.; Di Bari, L.; Zinna, F. Circularly Polarized Luminescence of Helicenes: A Data-Informed Insight. *Chirality* **2023**, *35* (4), 192–210. <https://doi.org/10.1002/chir.23535>.
- (25) Anderson, H. V.; Gois, N. D.; Chalifoux, W. A. New Advances in Chiral Nanographene Chemistry. *Org. Chem. Front.* **2023**, *10* (16), 4167–4197. <https://doi.org/10.1039/D3QO00517H>.
- (26) Vander Donckt, E.; Nasielski, J.; Greenleaf, J. R.; Birks, J. B. Fluorescence of the Helicenes. *Chem. Phys. Lett.* **1968**, *2* (6), 409–410. [https://doi.org/10.1016/0009-2614\(68\)80041-7](https://doi.org/10.1016/0009-2614(68)80041-7).
- (27) Kubo, H.; Hirose, T.; Matsuda, K. Control over the Emission Properties of [5]Helicenes Based on the Symmetry and Energy Levels of Their Molecular Orbitals. *Org. Lett.* **2017**, *19* (7), 1776–1779. <https://doi.org/10.1021/acs.orglett.7b00548>.
- (28) Teng, J.-M.; Zhang, D.-W.; Chen, C.-F. Recent Progress in Circularly Polarized Luminescence of [2.2]Paracyclophane Derivatives. *ChemPhotoChem* **2022**, *6* (3), e202100228. <https://doi.org/10.1002/cptc.202100228>.
- (29) Morisaki, Y.; Gon, M.; Sasamori, T.; Tokitoh, N.; Chujo, Y. Planar Chiral Tetrasubstituted [2.2]Paracyclophane: Optical Resolution and Functionalization. *J. Am. Chem. Soc.* **2014**, *136* (9), 3350–3353. <https://doi.org/10.1021/ja412197j>.
- (30) Tsuchiya, M.; Inoue, R.; Tanaka, K.; Morisaki, Y. Synthesis of Twisted Anthracenes: Induction of Twist Chirality by the Planar Chiral [2.2]Paracyclophane. *Chem. – Asian J.* **2022**, *17* (15), e202200418. <https://doi.org/10.1002/asia.202200418>.
- (31) Saal, F.; Zhang, F.; Holzapfel, M.; Stolte, M.; Michail, E.; Moos, M.; Schmiedel, A.; Krause, A.-M.; Lambert, C.; Würthner, F.; Ravat, P. [N]Helicene Diimides (n = 5, 6, and 7): Through-Bond versus Through-Space Conjugation. *J. Am. Chem. Soc.* **2020**, *142* (51), 21298–21303. <https://doi.org/10.1021/jacs.0c11053>.
- (32) Liu, B.; Böckmann, M.; Jiang, W.; Doltsinis, N. L.; Wang, Z. Perylene Diimide-Embedded Double [8]Helicenes. *J. Am. Chem. Soc.* **2020**, *142* (15), 7092–7099. <https://doi.org/10.1021/jacs.0c00954>.
- (33) Dhbaibi, K.; Favereau, L.; Srebro-Hooper, M.; Quinton, C.; Vanthuyne, N.; Arrico, L.; Roisnel, T.; Jamoussi, B.; Poriel, C.; Cabanetos, C.; Autschbach, J.; Crassous, J. Modulation of Circularly Polarized Luminescence through Excited-State Symmetry Breaking and Interbranched Exciton Coupling in Helical Push–Pull Organic Systems. *Chem. Sci.* **2020**, *11* (2), 567–576. <https://doi.org/10.1039/C9SC05231C>.
- (34) Mori, T. Chiroptical Properties of Symmetric Double, Triple, and Multiple Helicenes. *Chem. Rev.* **2021**, *121* (4), 2373–2412. <https://doi.org/10.1021/acs.chemrev.0c01017>.
- (35) Dhbaibi, K.; Abella, L.; Meunier-Della-Gatta, S.; Roisnel, T.; Vanthuyne, N.; Jamoussi, B.; Pieters, G.; Racine, B.; Quesnel, E.; Autschbach, J.; Crassous, J.; Favereau, L. Achieving High Circularly Polarized Luminescence with Push–Pull Helicenic Systems: From Rationalized Design to Top-Emission CP-OLED Applications. *Chem. Sci.* **2021**, *12* (15), 5522–5533. <https://doi.org/10.1039/D0SC06895K>.
- (36) Medel, M. A.; Tapia, R.; Blanco, V.; Miguel, D.; Morcillo, S. P.; Campaña, A. G. Octagon-Embedded Carbohelicene as a Chiral Motif for Circularly Polarized Luminescence Emission of Saddle-Helix Nanographenes. *Angew. Chem. Int. Ed.* **2021**, *60* (11), 6094–6100. <https://doi.org/10.1002/anie.202015368>.
- (37) Míguez-Lago, S.; Mariz, I. F. A.; Medel, M. A.; Cuerva, J. M.; Maçôas, E.; Cruz, C. M.; Campaña, A. G. Highly Contorted Superhelicene Hits Near-Infrared Circularly Polarized Luminescence. *Chem. Sci.* **2022**, *13* (35), 10267–10272. <https://doi.org/10.1039/D2SC03452B>.
- (38) Saal, F.; Swain, A.; Schmiedel, A.; Holzapfel, M.; Lambert, C.; Ravat, P. Push–Pull [7]Helicene Diimide: Excited-State Charge Transfer and Solvatochromic Circularly Polarized Luminescence. *Chem. Commun.* **2023**, *59* (94), 14005–14008. <https://doi.org/10.1039/D3CC04470J>.
- (39) Swain, A.; Radacki, K.; Braunschweig, H.; Ravat, P. Helically Twisted Nanoribbons via Stereospecific Annulative  $\pi$ -Extension Reaction Employing [7]Helicene as a Molecular Wrench. *Chem. Sci.* **2024**, *15* (30), 11737–11747. <https://doi.org/10.1039/D4SC01814A>.
- (40) Zhang, Y.; Guan, J.; Luo, L.; Han, X.; Wang, J.; Zheng, Y.; Xu, J. Chiral Twisted Molecular Carbons: Synthesis, Properties, and Applications. *Interdiscip. Mater.* **2024**, *3* (4), 453–479. <https://doi.org/10.1002/idm2.12173>.
- (41) Chen, J.-F.; Gao, Q.-X.; Yao, H.; Shi, B.; Zhang, Y.-M.; Wei, T.-B.; Lin, Q. Recent Advances in Circularly Polarized Luminescence of Planar Chiral Organic Compounds. *Chem. Commun.* **2024**, *60* (53), 6728–6740. <https://doi.org/10.1039/D4CC01698J>.
- (42) Kovida, K.; Malinčik, J.; M. Cruz, C.; G. Campaña, A.; Šolomek, T. Role of Exciton Delocalization in Chiroptical Properties of Benzothiadiazole Carbon Nanofoams. *Chem. Sci.* **2025**, *16* (3), 1405–1410. <https://doi.org/10.1039/D4SC07333A>.
- (43) Wu, Y.; Zhuang, G.; Cui, S.; Zhou, Y.; Wang, J.; Huang, Q.; Du, P. Through-Space  $\pi$ -Delocalization in a Conjugated Macrocyclic Consisting of [2.2]Paracyclophane. *Chem. Commun.* **2019**, *55* (97), 14617–14620. <https://doi.org/10.1039/C9CC06492C>.
- (44) He, J.; Yu, M.; Pang, M.; Fan, Y.; Lian, Z.; Wang, Y.; Wang, W.; Liu, Y.; Jiang, H. Nanosized Carbon Macrocycles Based on a Planar Chiral Pseudo Meta-[2.2]Paracyclophane. *Chem. – Eur. J.* **2022**, *28* (13), e202103832. <https://doi.org/10.1002/chem.202103832>.
- (45) Malinčik, J.; Cruz, C. M.; Campaña, A. G.; Šolomek, T.  $\pi$ -System Bistability Determines the Circularly Polarized Luminescence in Helicene Para-Phenylenes. ChemRxiv February 7, 2024. <https://doi.org/10.26434/chemrxiv-2024-6pxt4>.

- (46) Rivera-Fuentes, P.; Alonso-Gómez, J. L.; Petrovic, A. G.; Seiler, P.; Santoro, F.; Harada, N.; Berova, N.; Rzepa, H. S.; Diederich, F. Enantiomerically Pure Allenone–Acetylenic Macrocycles: Synthesis, Solid-State Structures, Chiroptical Properties, and Electron Localization Function Analysis. *Chem. – Eur. J.* **2010**, *16* (32), 9796–9807. <https://doi.org/10.1002/chem.201001087>.
- (47) Sato, S.; Yoshii, A.; Takahashi, S.; Furumi, S.; Takeuchi, M.; Isobe, H. Chiral Intertwined Spirals and Magnetic Transition Dipole Moments Dictated by Cylinder Helicity. *Proc. Natl. Acad. Sci.* **2017**, *114* (50), 13097–13101. <https://doi.org/10.1073/pnas.1717524114>.
- (48) Wang, J.; Zhuang, G.; Chen, M.; Lu, D.; Li, Z.; Huang, Q.; Jia, H.; Cui, S.; Shao, X.; Yang, S.; Du, P. Selective Synthesis of Conjugated Chiral Macrocycles: Sidewall Segments of (-)/(+)-(12,4) Carbon Nanotubes with Strong Circularly Polarized Luminescence. *Angew. Chem. Int. Ed.* **2020**, *59* (4), 1619–1626. <https://doi.org/10.1002/anie.201909401>.
- (49) Hasegawa, M.; Nojima, Y.; Mazaki, Y. Circularly Polarized Luminescence in Chiral  $\pi$ -Conjugated Macrocycles. *ChemPhotoChem* **2021**, *5* (12), 1042–1058. <https://doi.org/10.1002/cptc.202100162>.
- (50) Tanaka, H.; Ikenosako, M.; Kato, Y.; Fujiki, M.; Inoue, Y.; Mori, T. Symmetry-Based Rational Design for Boosting Chiroptical Responses. *Commun. Chem.* **2018**, *1* (1), 1–8. <https://doi.org/10.1038/s42004-018-0035-x>.
- (51) Kubo, H.; Shimizu, D.; Hirose, T.; Matsuda, K. Circularly Polarized Luminescence Designed from Molecular Orbitals: A Figure-Eight-Shaped [5]Helicene Dimer with D<sub>2</sub> Symmetry. *Org. Lett.* **2020**, *22* (23), 9276–9281. <https://doi.org/10.1021/acs.orglett.0c03506>.
- (52) Uceda, R. G.; Cruz, C. M.; Míguez-Lago, S.; de Cienfuegos, L. Á.; Longhi, G.; Pelta, D. A.; Novoa, P.; Mota, A. J.; Cueva, J. M.; Miguel, D. Can Magnetic Dipole Transition Moment Be Engineered? *Angew. Chem. Int. Ed.* **2024**, *63* (4), e202316696. <https://doi.org/10.1002/anie.202316696>.
- (53) Gelessus, A.; Thiel, W.; Weber, W. Multipoles and Symmetry. *J. Chem. Educ.* **1995**, *72* (6), 505. <https://doi.org/10.1021/ed072p505>.
- (54) Kovida, K.; Malinčák, J.; Cruz, C. M.; Campaña, A. G.; Šolomek, T. Red-Shifted Circularly Polarized Luminescence in Chiral Planar Benzothiadiazole Carbon Nanohoop. ChemRxiv November 30, 2023. <https://doi.org/10.26434/chemrxiv-2023-vs2q>.
- (55) Lovell, T. C.; Garrison, Z. R.; Jasti, R. Synthesis, Characterization, and Computational Investigation of Bright Orange-Emitting Benzothiadiazole [10]Cycloparaphenylene. *Angew. Chem. Int. Ed.* **2020**, *59* (34), 14363–14367. <https://doi.org/10.1002/anie.202006350>.
- (56) Malinčák, J.; Gaikwad, S.; Mora-Fuentes, J. P.; Boillat, M.-A.; Prescimone, A.; Häussinger, D.; Campaña, A. G.; Šolomek, T. Circularly Polarized Luminescence in a Möbius Helicene Carbon Nanohoop\*\*. *Angew. Chem. Int. Ed.* **2022**, *61* (37), e202208591. <https://doi.org/10.1002/anie.202208591>.
- (57) Yang, H.; Guo, S.; Guo, W.; Liu, L.; Liu, X.; He, J.; Fan, Y.; Lian, Z.; Li, X.; Huang, S.; Chen, X.; Wang, Y.; Jiang, H. Neutral and Dicationic [5]Helicene-Embedded Cycloparaphenylene Nanohoops with Möbius Topology and Local/In-Plane Aromaticity. ChemRxiv October 29, 2024. <https://doi.org/10.26434/chemrxiv-2024-vxf63-v2>.
- (58) Jhulki, S.; Mishra, A. K.; Chow, T. J.; Moorthy, J. N. Helicenes as All-in-One Organic Materials for Application in OLEDs: Synthesis and Diverse Applications of Carbo- and Aza[5]Helical Diamines. *Chem. – Eur. J.* **2016**, *22* (27), 9375–9386. <https://doi.org/10.1002/chem.201600668>.
- (59) Sisto, T. J.; Golder, M. R.; Hirst, E. S.; Jasti, R. Selective Synthesis of Strained [7]Cycloparaphenylene: An Orange-Emitting Fluorophore. *J. Am. Chem. Soc.* **2011**, *133* (40), 15800–15802. <https://doi.org/10.1021/ja205606p>.
- (60) Kręćjasz, R. B.; Malinčák, J.; Šolomek, T. Exploring Silyl Protecting Groups for the Synthesis of Carbon Nanohoops. *Synthesis* **2023**, *55* (9), 1355–1366. <https://doi.org/10.1055/a-2008-9505>.
- (61) Patel, V. K.; Kayahara, E.; Yamago, S. Practical Synthesis of [n]Cycloparaphenylenes (N=5, 7–12) by H<sub>2</sub>SnCl<sub>4</sub>-Mediated Aromatization of 1,4-Dihydroxycyclo-2,5-Diene Precursors. *Chem. – Eur. J.* **2015**, *21* (15), 5742–5749. <https://doi.org/10.1002/chem.201406650>.
- (62) Segawa, Y.; Fukazawa, A.; Matsuura, S.; Omachi, H.; Yamaguchi, S.; Irle, S.; Itami, K. Combined Experimental and Theoretical Studies on the Photophysical Properties of Cycloparaphenylenes. *Org. Biomol. Chem.* **2012**, *10* (30), 5979–5984. <https://doi.org/10.1039/C2OB25199J>.
- (63) Darzi, E. R.; Jasti, R. The Dynamic, Size-Dependent Properties of [5]–[12]Cycloparaphenylenes. *Chem. Soc. Rev.* **2015**, *44* (18), 6401–6410. <https://doi.org/10.1039/C5CS00143A>.
- (64) Lovell, T. C.; Colwell, C. E.; Zakharov, L. N.; Jasti, R. Symmetry Breaking and the Turn-on Fluorescence of Small, Highly Strained Carbon Nanohoops. *Chem Sci* **2019**, *10* (13), 3786–3790. <https://doi.org/10.1039/C9SC00169G>.
- (65) Darzi, E. R.; Hirst, E. S.; Weber, C. D.; Zakharov, L. N.; Lonergan, M. C.; Jasti, R. Synthesis, Properties, and Design Principles of Donor–Acceptor Nanohoops. *ACS Cent. Sci.* **2015**, *1* (6), 335–342. <https://doi.org/10.1021/acscentsci.5b00269>.
- (66) Raden, J. M. V.; Darzi, E. R.; Zakharov, L. N.; Jasti, R. Synthesis and Characterization of a Highly Strained Donor–Acceptor Nanohoop. *Org. Biomol. Chem.* **2016**, *14* (24), 5721–5727. <https://doi.org/10.1039/C6OB00133E>.

- (67) Lovell, T. C.; Fosnacht, K. G.; Colwell, C. E.; Jasti, R. Effect of Curvature and Placement of Donor and Acceptor Units in Cycloparaphenylenes: A Computational Study. *Chem. Sci.* **2020**, *11* (44), 12029–12035. <https://doi.org/10.1039/D0SC03923C>.
- (68) Weiland, K. J.; Brandl, T.; Atz, K.; Prescimone, A.; Häussinger, D.; Šolomek, T.; Mayor, M. Mechanical Stabilization of Helical Chirality in a Macrocyclic Oligothiophene. *J. Am. Chem. Soc.* **2019**, *141* (5), 2104–2110. <https://doi.org/10.1021/jacs.8b11797>.
- (69) Frisch, M. J.; Trucks, G. W.; Schlegel, H. B.; Scuseria, G. E.; Robb, M. A.; Cheeseman, J. R.; Scalmani, G.; Barone, V.; Petersson, G. A.; Nakatsuji, H.; Li, X.; Caricato, M.; Marenich, A. V.; Bloino, J.; Janesko, B. G.; Gomperts, R.; Mennucci, B.; Hratchian, H. P.; Ortiz, J. V.; Izmaylov, A. F.; Sonnenberg, J. L.; Williams, Ding, F.; Lipparini, F.; Egidi, F.; Goings, J.; Peng, B.; Petrone, A.; Henderson, T.; Ranasinghe, D.; Zakrzewski, V. G.; Gao, J.; Rega, N.; Zheng, G.; Liang, W.; Hada, M.; Ehara, M.; Toyota, K.; Fukuda, R.; Hasegawa, J.; Ishida, M.; Nakajima, T.; Honda, Y.; Kitao, O.; Nakai, H.; Vreven, T.; Throssell, K.; Montgomery Jr., J. A.; Peralta, J. E.; Ogliaro, F.; Bearpark, M. J.; Heyd, J. J.; Brothers, E. N.; Kudin, K. N.; Staroverov, V. N.; Keith, T. A.; Kobayashi, R.; Normand, J.; Raghavachari, K.; Rendell, A. P.; Burant, J. C.; Iyengar, S. S.; Tomasi, J.; Cossi, M.; Millam, J. M.; Klene, M.; Adamo, C.; Cammi, R.; Ochterski, J. W.; Martin, R. L.; Morokuma, K.; Farkas, O.; Foresman, J. B.; Fox, D. J. Gaussian 16 Rev. C.02, 2016.